



St3TART

FRM for Sentinel-3 Land Altimetry

Sentinel-3 Topography mission Assessment through Reference Techniques (St3TART)

TD-13_2: FRM Campaign Final Report - Sea-ice

	Function	Name	Signature	Date
Prepared by	St3TART Project Team	Henriette Skourup, Sara Fleury, Jean-Christophe Poisson, Valentin Fouqueau, Frederic Vivier & Antonio Lourenço	<i>p.o.</i> 	17/04/23
Approved by	Project manager	Elodie Da Silva		17/04/23
Authorized by	Deputy CEO	Mahmoud EL HAJJ		17/04/23
Accepted by	ESA Technical Project Officer	Pierre FEMENIAS		

SENTINEL-3 TOPOGRAPHY MISSION ASSESSMENT THROUGH REFERENCE TECHNIQUES (St3TART)	Ref	NOV-FE-0899-NT-102		
	Issue	2	Date	03/04/23
	Rev	1	Date	17/04/23
	Page	2/55		

Distribution list

INTERNAL	EXTERNAL	
Name	Name	Company / Organisation
NOVELTIS Documentation	Mr. Pierre FÉMÉNIAS	ESA
Mr. Richard BRU	Mr. Jérôme BOUFFARD	ESA
Mr. Mahmoud EL HAJJ	Mr. Philippe GORYL	ESA
St3TART Project team	Ms Filomena CATAPANO	RHEA for ESA

Ref	NOV-FE-0899-NT-102		
Issue	2	Date	03/04/23
Rev	1	Date	17/04/23
Page	3/55		

Document status

Sentinel-3 Topography mission Assessment through Reference Techniques (St3TART)			
TD-13_2: FRM Campaign Final Report - Sea-ice			
Issue	Revision	Date	Reason for the revision
1	0	20/01/2023	Initial version
2	0	31/03/2023	Revised version according to #PM3 ESA review
2	1	18/04/2023	Revised according to Final ESA review - minor changes

Modification status				
Issue	Rev	Status *	Modified pages	Reason for the modification
2	0	M	All	Revised version according to #PM3 ESA review
2	1	M D M M I I		Revised according to Final ESA review - minor changes Section 2.4 Figures 17 and 41 Paragraph above Figure 46 Figure 49 a better description has been added Figure 51 has been added to better compare SIMS and drone-lidar measure

* *I = Inserted D = Deleted M = Modified*

Acronyms

The acronyms used in this document are defined in [RD5].

Reference documents

N°	Reference	Title
[RD1]	ESA-EOPG-CSCOP-SOW-29, Issue 1 Rev. 4 – 28/10/2020	Statement of Work - Sentinel-3 Topography mission Assessment through Reference Techniques (St3TART)
[RD2]	NOV-FE-0899-PR-002	Technical Proposal
[RD3]	NOV-FE-0899-PR-004	Implementation Proposal
[RD4]	ESA Contract No. 4000135181/21/I-DT	ESA Contract – Copernicus ground segment Sentinel-3 Topography mission Assessment through Reference Techniques (St3TART)
[RD5]	NOV-FE-0899-NT-040	Acronyms list
[RD6]	Rolf Ole R. Jenssen & Svein Jacobsen (2020) Drone-mounted UWB snow radar: technical improvements and field results, Journal of Electromagnetic Waves and Applications, 34:14, 1930-1954, DOI: 10.1080/09205071.2020.1799871	
[RD7]	R. O. R. Jenssen, M. Eckerstorfer and S. Jacobsen, "Drone-Mounted Ultrawideband Radar for Retrieval of Snowpack Properties," in IEEE Transactions on Instrumentation and Measurement, vol. 69, no. 1, pp. 221-230, Jan. 2020, doi: 10.1109/TIM.2019.2893043	

Ref	NOV-FE-0899-NT-102		
Issue	2	Date	03/04/23
Rev	1	Date	17/04/23
Page	5/55		

Table of contents

1. INTRODUCTION.....	6
1.1. PURPOSE AND SCOPE	6
1.2. OVERVIEW OF THIS DOCUMENT	6
2. THE SATELLITE VALIDATION APPROACH.....	7
2.1. ICE-T BUOY.....	7
2.2. AIRBORNE DATA	7
2.3. DRONE	8
3. CAMPAIGN DATA DESCRIPTION	9
3.1. DRONE EXPERIMENT - LAND-BASED (VORTEX.IO)	9
3.1.1. <i>Campaign log</i>	10
3.1.2. <i>Precise positioning</i>	11
3.1.3. <i>Quality of lidar measurements</i>	14
3.1.4. <i>Sea ice surface analysis</i>	16
3.1.5. <i>Conclusion of the drone campaign</i>	23
3.2. ICE-T BUOY (LOCEAN)	24
3.2.1. <i>Sea ice thickness</i>	27
3.2.2. <i>Snow experiment</i>	31
3.3. AIRBORNE DATA	35
3.3.1. <i>Sea ice freeboards from lidar</i>	35
3.3.2. <i>Sea ice freeboard from Ku/Ka-band radar altimeters</i>	36
3.3.3. <i>Surface classification from visual images</i>	37
3.4. DRONE FROM SHIP (LEGOS)	38
3.4.1. <i>Description of the datasets</i>	38
3.4.2. <i>Freeboard processing from lidar datasets</i>	43
3.4.3. <i>Discussion</i>	51
4. COMPARISON OF S3 DATA TO CAMPAIGN DATA	52
5. CONCLUSIONS.....	53
5.1. AIRBORNE MEASUREMENTS	53
5.2. ICE-T MEASUREMENTS	53
5.3. DRONE MEASUREMENTS	54
5.4. OTHER TECHNIQUES OF MEASUREMENTS	55
5.5. OVERALL CONCLUSION	55

SENTINEL-3 TOPOGRAPHY MISSION ASSESSMENT THROUGH REFERENCE TECHNIQUES (St3TART)	Ref	NOV-FE-0899-NT-102		
	Issue	2	Date	03/04/23
	Rev	1	Date	17/04/23
	Page	6/55		

1. Introduction

1.1. Purpose and scope

This document is the FRM Campaign Final Report for the “Sentinel-3 Topography mission Assessment through Reference Techniques (St3TART)” project, [RD1].

It describes the satellite validation approach, the uncertainty estimation and budget, the results obtained, as well as the findings/conclusions following all the realized campaigns.

1.2. Overview of this document

In addition to this Introduction chapter, this FRM campaign final report includes the following chapters:

- § 2, The satellite validation approach
- § 3, Campaign data description
- § 4, Comparison of S3 to campaign data
- § 5, Conclusions

New processors for Sentinel-3 thematic products are being developed in the framework of the S3 MPC project led by CLS, for sea ice, land ice and hydrology products. It will represent an important progress as for now the common processing chain does not include zero-padding and Hammer filtering, which are crucial for SAR processing over sea ice covered regions. These have already been implemented in a pilot processing, but it does not yet include data prior to June 2022. On December 21 2022 we have requested a re-processing of dedicated Sentinel-3 orbits under-flown during the St3TART 2022 spring campaign using this new baseline, and hope these will be available before the final meeting, April 20 2023, and in time to make a comparison with the campaign data. We have added some examples in Chapter 2.

The requested tracks are:

- Sentinel-3A 27-03-2022 15:51
'S3A_SR_2_WAT____20220327T154634_20220327T163326_20220422T080327_2812_083_268_____MAR_
O_NT_004.SEN3'
 - cycle_number = 83
 - absolute_rev_number = 31811
 - pass_number = 536
 - absolute_pass_number = 63622
- Sentinel-3A 28-03-2022 00:07
'S3A_SR_2_WAT____20220327T232600_20220328T001129_20220422T153630_2729_083_272_____MAR_
O_NT_004.SEN3'
 - cycle_number = 83
 - absolute_rev_number = 31815
 - pass_number = 545
 - absolute_pass_number = 63631
- Sentinel-3B 30-03-2022 23:51
'S3B_SR_2_WAT____20220330T230902_20220330T235429_20220425T153636_2727_064_172_____MAR_
O_NT_004.SEN3'
 - cycle_number = 64
 - absolute_rev_number = 20464
 - pass_number = 345
 - absolute_pass_number = 40929

2. The satellite validation approach

Here we provide some descriptions and examples of how we expect to do the satellite validation using the campaign data based on similar collected campaign data and comparisons with CryoSat-2.

2.1. Ice-T buoy

The Ice-T buoy is directly collocated to the satellite passes within a given distance and time from the buoy's position. The measurand would be the SIT. Currently, there is no SIT in the S3 baseline, nor any contributing information about snow depth, sea ice, water or snow densities to use in our computation of S3 radar freeboard to S3 SIT. Common procedures would consist in using the information provided in the satellite product to calculate the measurand, here the SIT. In this case, where the auxiliary data are not available in the satellite product, we would simply use the S3 radar freeboard and compute the associated S3 SIT using information of snow depth, and the densities obtained by the Ice-T buoy and the associated in situ measurements made during the deployment of the buoy. The comparison is derived by computing the median and standard deviation of the satellite SIT within the collocation disc, where the standard deviation is crucial, to have an estimate of spatial variability for comparison with a point measurement. An example is provided in Figure 1.

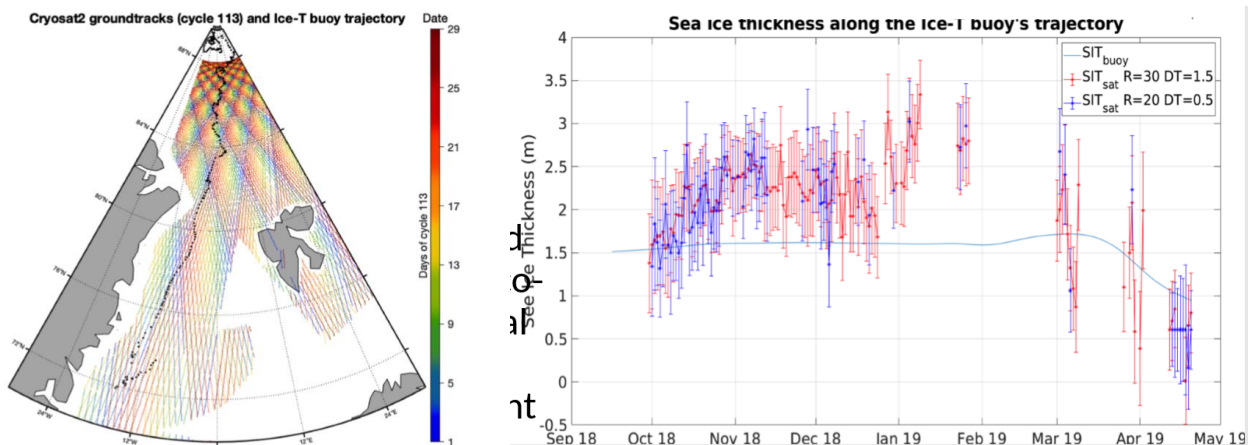


Figure 1 - Example of the Ice-T buoy trajectory and CryoSat-2 ground tracks from a cycle color-coded by the days of the cycle (left) and associated SIT comparison.

2.2. Airborne data

As described in TD-2 section 7.4, there are 2 approaches for the inter-comparison of satellite and airborne data;

- 1) Along-track used for underflights (TD-2 Section 7.4.1.1.4)
- 2) Gridded (TD-2 Section 7.4.1.1.4)

Both approaches are demonstrated in Figure 2.

As we did underfly several S3 orbits trajectories during the St3TART spring campaign we intend to use the along-track approach. To compare the airborne freeboards to the S3, we would need to make an adjustment for the sea ice drift as the satellite and airborne data are not acquired at the same time. This is first of all caused by the differences in the aircraft and satellite surface speeds. What takes the satellite 1-2 seconds to cover, takes 4-5 hours for an aircraft with ground speeds of 250 km/h. Other causes depend on the weather and possible resulting delays, on airport opening hours and on priorities.

Ref	NOV-FE-0899-NT-102		
Issue	2	Date	03/04/23
Rev	1	Date	17/04/23
Page	8/55		

The drift corrections can be applied by using different approaches:

- 1) input from the drift of the Ice-T buoy,
- 2) use of auto-correlation functions,
- 3) manual approach,
- 4) use of external drift products, i.e. from OSI-SAF and/or drift vectors extracted feature tracking from repeated SAR images.

The manual approach can only be used in cases of direct underflights with a low drift speed. The approach with the lowest uncertainty is by using drifting buoys, but it depends on the distance between the airborne measurement and the location of the buoy.

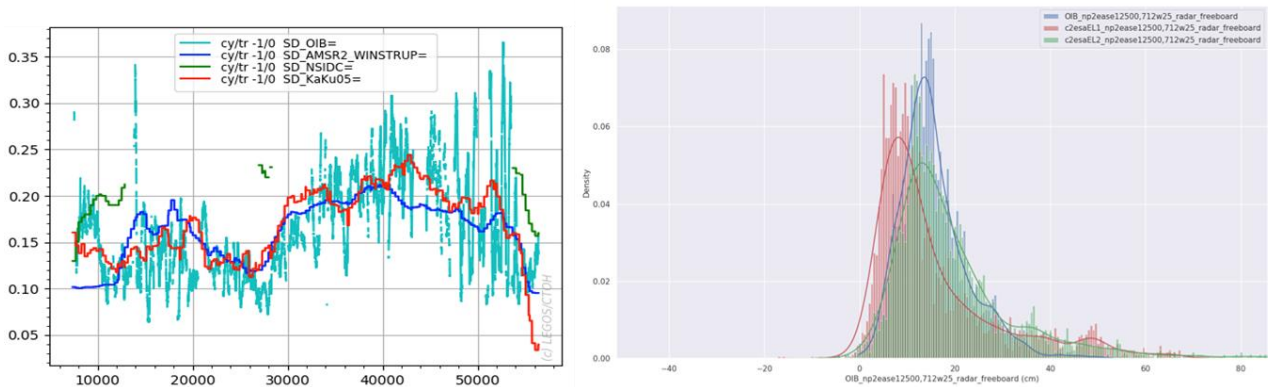


Figure 2 - Along-track intercomparison from airborne, satellites and models (left). Radar freeboard histograms from airborne and satellite CryoSat-2 using the gridded approach (right).

2.3. Drone

For the St3TART spring campaign drone data, we do not expect to provide comparison with S3, as there are unfortunately no overlapping data, due to delays imputable to weather and technical issues with the helicopter (see TD-12-2 FRM Campaign Log for Sea Ice). The aim is to provide local surveys over the satellite footprint area, i.e. 300m x 1600 m for S3 SAR, in a pattern of parallel flight lines to obtain sub-footprint information of freeboard topography and surface roughness on footprint scales.

3. Campaign data description

In this chapter we consolidate all the in-situ measurements carried out during the project. They include measurements obtained during the St3TART 2022 spring campaign in the Baffin Bay in Greenland (illustrated in Figure 3):

- Lidar and camera data from the drone experiment aimed at demonstrating its capabilities over sea ice
- Ice-T buoy sea ice thickness, and first results of the experimental snow depth miniature radars
- Sea ice freeboard and images from fixed winged multi-frequency airborne sensors ALS/Ku/Ka

In addition, we were given the opportunity to test a lidar equipped drone with a similar setup as the St3TART Baffin Bay campaign from a moving platform, namely the icebreaking cruise ship “Le Commandant Charcot” operated by the French shipping company “Compagnie du Ponant” during the summer 2022. First results from this campaign are also included here. The setup and general description of the campaigns are provided in the dedicated deliverables for the campaigns in “TD-12-2 Sea Ice FRM Campaign Logs”.

All the campaign data will be provided in the netcdf file format according TD-9 “FRM Data Hub File Name Convention and Format” and uploaded to the St3TART FRM data hub.

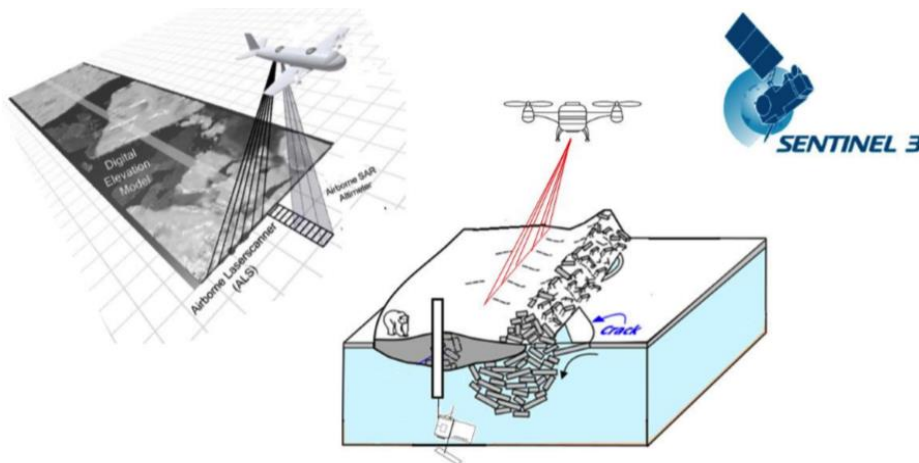


Figure 3 - The St3TART spring campaign setup with drone, Ice-T buoy, fixed winged aircraft and S3.

3.1. Drone experiment - land-based (vortex.io)

The use of drones for measuring sea ice is a new topic with great expectations in order to answer different issues of instrumentation deployment over sea ice: reduce costs, increase flexibility, enable the use of new types of instrumentation. This new Cal/Val means is complementary to existing solutions and will not replace airborne campaign or other in-situ means, but it will complete the range of in-situ Cal/Val solutions in order to fill the gap between airborne measurement and in-situ measurements in terms of spatio-temporal scales.

In this context, the deployment objectives of this campaign over Greenland were:

1. Test drone deployment with its associated instrumentation, the vortex.io lightweight LiDAR altimeter in extreme conditions (temperature < -10°C and windy conditions)
2. Evaluate the capability to compute a precise GNSS positioning needed for LiDAR altimetry in such high latitudes
3. Evaluate the quality of LiDAR measurements over sea ice (the LiDAR altimeter has never been used over sea ice surfaces)
4. Evaluate the capability to deploy a drone with all the equipment related to the use of the vortex.io LiDAR altimeter over sea ice with all the logistics issues implied.

Ref	NOV-FE-0899-NT-102		
Issue	2	Date	03/04/23
Rev	1	Date	17/04/23
Page	10/55		

Of course, this campaign was also focused on these science objectives:

1. Evaluate the capability and the precision of the drone embedded LiDAR altimeter to precisely measure the sea ice elevation (elevation over ice floes)
2. Evaluate the capability of the drone embedded LiDAR altimeter to measure sea ice freeboard
3. Evaluate the capability of the drone embedded LiDAR altimeter to be deployed below the Sentinel-3 track

3.1.1. Campaign log

The ESA St3TART sea ice campaign was coordinated with CryoVEx/CRYO2ICE/SILICE spring 2022 campaign, which took place March 21 – April 8, 2022 to share logistics.

Due to bad weather conditions, the drone team was not able to perform planned flights under the Sentinel-3 ground track on the sea ice far off the coast of Upernavik. 4 LiDAR acquisition flights have been performed, 2 during the first day of deployment (March 29, 2022) and 2 during the second day (March 30, 2022).

During the second day, 2 orthophoto flights have been performed on the same sites to have images of the sea ice surface. The sea ice close to the coast of Upernavik is fast ice and does not have the same characteristics as the drifting sea ice under the satellite ground track where we originally planned to test the drone. The observed leads were very narrow and full of floating ice (most likely leads created by small boats).

3.1.1.1. First day of measurement on March 29, 2022

2 flights were performed from Upernavik coast: 24 km travelled by the altimeter with a maximum of 3.5 km distance from the drone team at an altitude of 30 meters. The first flight overflew the area to observe the sea ice surface and locate leads in the sea ice. The second flight was performed to measure freeboard by overflying the leads and the interface between the sea ice and the free water as shown in Figure 4.

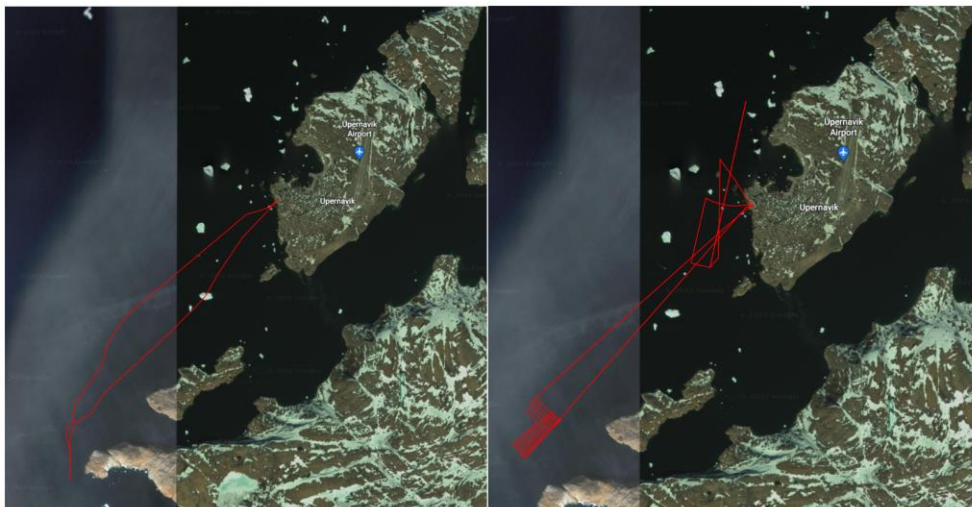


Figure 4 - On the left, map of the first flight performed on March 29, 2022. On the right, map of the second drone flight performed.

3.1.1.2. Second day of measurement on March 30, 2022

2 flights were performed from Upernavik coast: 36 km travelled by the altimeter to cover the areas and to overfly leads at an altitude of 20 meters. The first flight was performed just outside of the Upernavik bay to overfly leads in the area. The second flight flew over the same area as the previous day's flights to fly over leads. An orthophoto flight has been performed on each area to get a precise image of the sea ice surface. These flights were performed at an altitude of 100 meters to increase the overlap between each drone picture. All drone trajectories are shown in Figure 5.

Ref	NOV-FE-0899-NT-102		
Issue	2	Date	03/04/23
Rev	1	Date	17/04/23
Page	11/55		

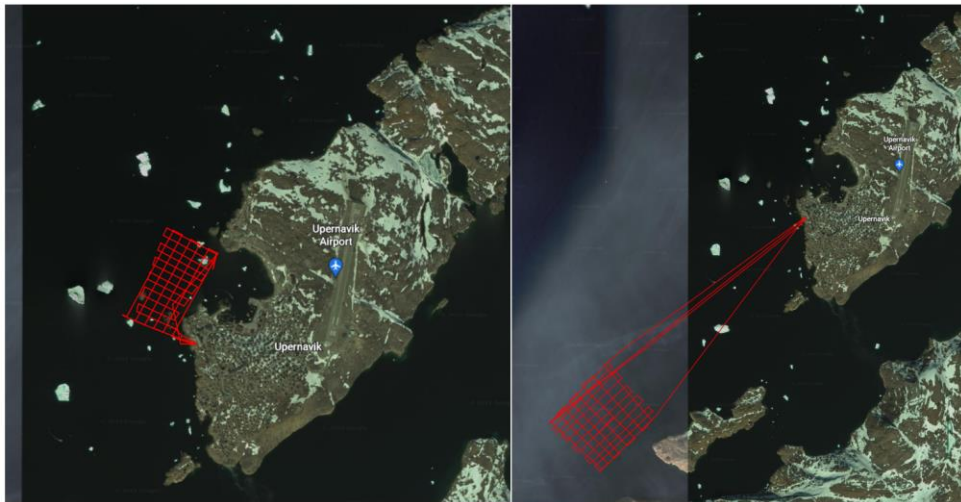


Figure 5 - On the left, drone trajectory of the first flight. On the right, the drone trajectory of the second flight.

3.1.2. Precise positioning

3.1.2.1. GNSS base precise positioning

The first step in the processing of the drone embedded LiDAR data is to compute the precise positioning of the altimeter during all the drone flight. To do so, we performed a GNSS Post Processing Kinematic (PPK) which precisely positioned the altimeter with respect to the GNSS base. It is a precise relative positioning. To obtain an absolute precise positioning we must first compute the GNSS base position. To do so, a GNSS Precise Point Positioning processing (PPP) is applied to the raw RINEX data recorded from the Septentrio NR3 base. We used final orbit products from the GRGS (Groupe de Recherche de Géodésie Spatiale) as well as clock and ephemeris products.

The base positioning results for the first day are presented in Figure 6.

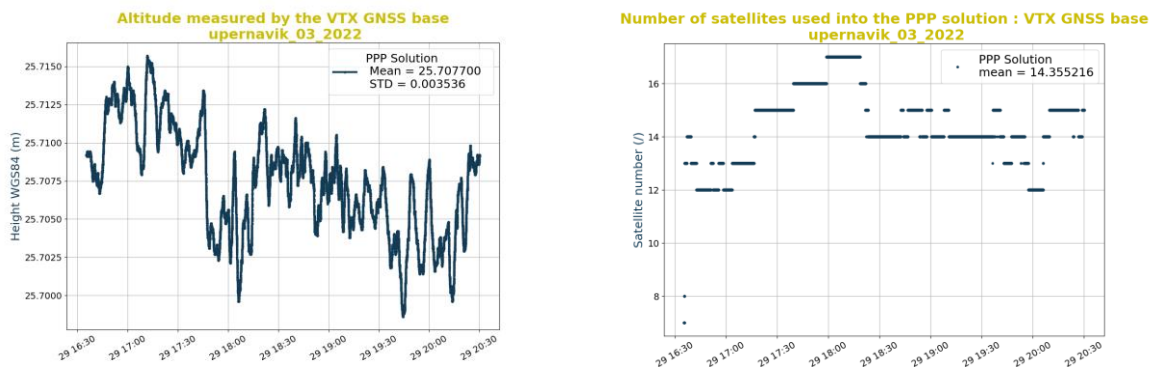


Figure 6 - On the left, computed ellipsoidal elevation of the GNSS base on the first day (March 29, 2022). On the right, number of GNSS satellites used for the PPP solution on the first day

The performances of the positioning are very good, with a standard deviation of the elevation of 3.5 mm during the day and an average of 14.5 tracked GNSS satellites (GPS + GLONASS + GALILEO), knowing that the base did not move at all during the day (static position on a tripod).

The base positioning results for the first day are presented in Figure 7.

Ref	NOV-FE-0899-NT-102		
Issue	2	Date	03/04/23
Rev	1	Date	17/04/23
Page	12/55		

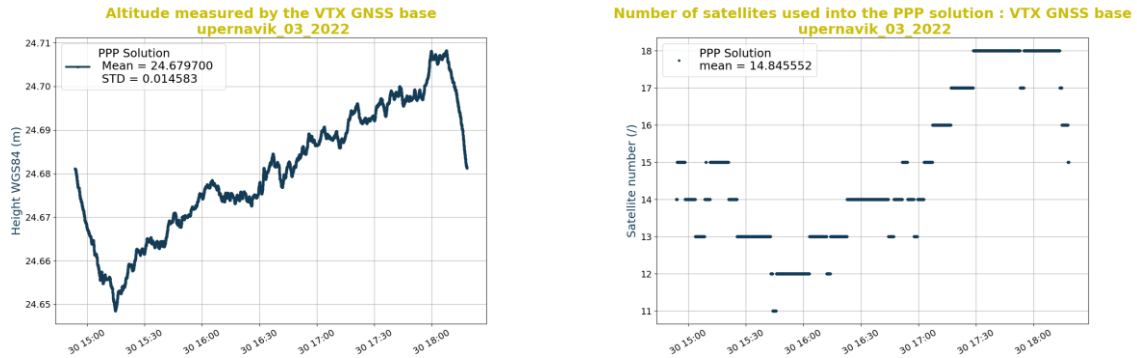


Figure 7 - On the left, computed ellipsoidal elevation of the GNSS base on the second day (March 30, 2022). On the right, number of GNSS satellites used for the PPP solution on the second day

On the second day, the GNSS base was not installed on solid ground by the drone team unfortunately but directly on the sea ice (at just a few centimetres from the coast). It results in a moving GNSS base elevation (w.r.t the reference ellipsoid) which leads to a standard deviation of 1.45 cm during the day. The number of tracked GNSS satellites is very good with an average of 14.84.

3.1.2.2. LiDAR altimeter precise positioning

On the first day, raw GNSS measurements recorded by the on-board GNSS receiver (Septentrio) during the two flights performed have been processed using a GNSS PPK processing. The resulting positioning presents excellent performances for the 2 days with 99% of ambiguities fixed during the measurement part of the flights. Results are presented in Figure 8 for the 2 flights performed on the first day and in Figure 9 for the 2 flights performed on the second day. The green dots represent a GNSS positioning solution with fixed ambiguities (best accuracy) whereas red dots correspond to a GNSS positioning solution with floating ambiguities (lower accuracy).

Ref	NOV-FE-0899-NT-102		
Issue	2	Date	03/04/23
Rev	1	Date	17/04/23
Page	13/55		

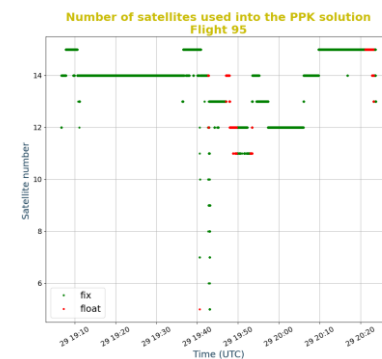
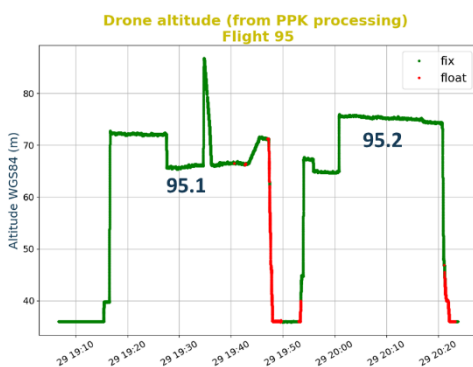
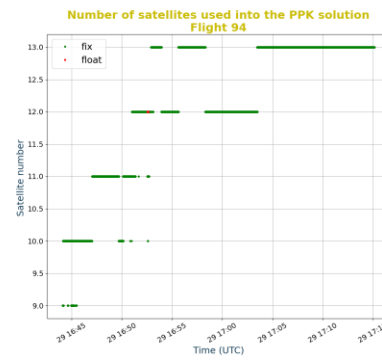
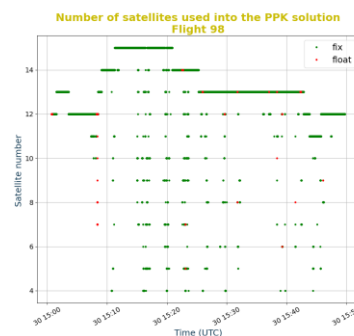
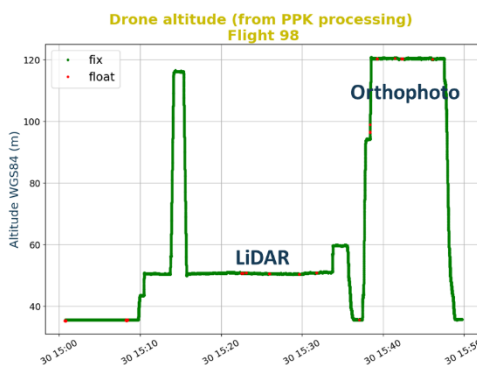


Figure 8 - On top left, elevation of the drone embedded LIDAR altimeter during the first flight on March 29, 2022. Top right: number of GNSS satellites tracked during the first flight. Bottom left: elevation of the LIDAR altimeter during the second flight. Bottom right: number of GNSS satellites tracked during the second flight.

On the first day, the positioning performances are excellent for the first flight and good for the second flight. Indeed, even if some floating ambiguities can be observed in the second flight these points are in take-off and landing phases (with very few points during LIDAR measurements that have been easily edited). On the second day, the first flight shows very good quality with near 98% of fixed ambiguities. The few points with floating ambiguities are directly edited. For the second flight, the performances are not excellent but are still totally exploitable. In this case, points with floating ambiguities will be looked carefully and the impact on the elevation retrieval will be analysed before being edited.



Ref	NOV-FE-0899-NT-102		
Issue	2	Date	03/04/23
Rev	1	Date	17/04/23
Page	14/55		

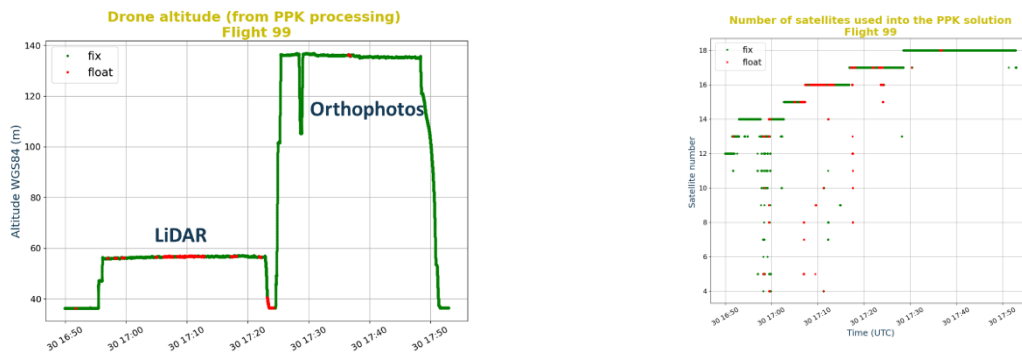


Figure 9 - On top left, elevation of the drone embedded LiDAR altimeter during the first flight on March 30, 2022. Top right: number of GNSS satellites tracked during the first flight. Bottom left: elevation of the LiDAR altimeter during the second flight. Bottom right: number of GNSS satellites tracked during the second flight.

3.1.2.3. Conclusion about precise positioning

The base positioning is excellent for both days even with a small mistake in the base installation during the second day, where it was placed on the sea ice. Almost all ambiguities are fixed during the flights, the positioning of all the flights is fully exploitable. Ambiguities are not always fixed during take-off and landing phases, but this is not an issue since these parts of the flights are not used for computing the surface elevation. We observed some losses of radio connection between the drone and the remote control. This is not an issue since the connection came back and the flight program restarted where it stopped. These connection losses are not a surprise in such an environment at such a distance (almost 4 km between the remote control and the drone).

In conclusion, we can safely say that the precise positioning is good during the whole campaign which is one of the objectives of this campaign.

3.1.3. Quality of lidar measurements

3.1.3.1. First day of measurement on March 29, 2022

Figure 10 presents the percentage of edited measurements per LiDAR beam (the vortex.io LiDAR altimeter has 8 beams spread out on a swath of 16.3°) during the first flight of the first deployment day. This figure shows a high number of edited data on all beams, between 45% and 65%. This high percentage is due to an abnormally high mispointing angle as shown by the 2 histograms (roll angle and pitch angle) presented in Figure 11. The average angle in both directions is close to 2° which is the consequence of issues during the gyro-pod calibration phase. The gyro-pod is a UAV servo system that maintains the altimeter with a Nadir pointing. An issue in the calibration can lead to bad nadir pointing as observed on this flight.

Since the LiDAR altimeter has 8 beams distributed into the across-track direction, a high roll angle is not an issue as long as the roll angle value is below the swath angle (+/- 8.2°). On the other hand, a high pitch angle is more problematic since the beam width in the along-track direction is 2°. We can see here that a pitch angle of 2° is too important and is the main reason for the high percentage of edited measurements.

The drone team analysed the data on the field and then corrected the calibration of the gyro-system for all the other flights.

Ref	NOV-FE-0899-NT-102		
Issue	2	Date	03/04/23
Rev	1	Date	17/04/23
Page	15/55		

**Percentage of missed measure per beam, flight 94.1
Upernavik 03/2022**

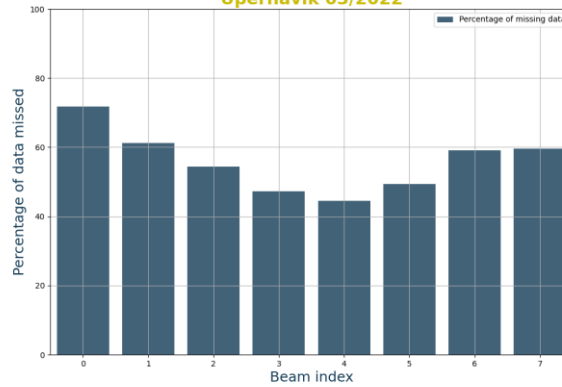


Figure 10 - Percentage of edited measure per beam during the first flight of the first deployment day

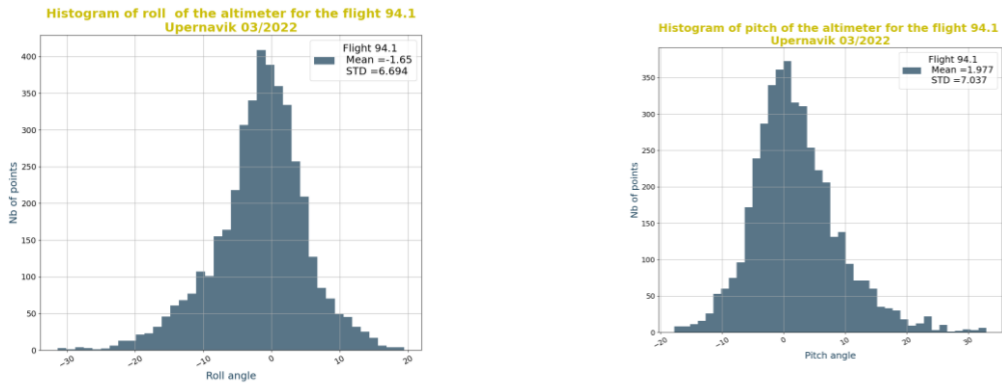


Figure 11 - Histograms of the roll angle (on the left) and the pitch angle (on the right) measured by the internal Inertial Measurement Unit (IMU) integrated into the vortex.io LiDAR altimeter

Since this correction, all other flights performed on the first day show a very low percentage (between ~20% and ~35% at maximum) of edited value, which demonstrates a very good backscattering of the LiDAR above sea ice (as expected due to the rough surface). The percentage of edited data for the 2 other LiDAR acquisitions performed on this day are presented in Figure 12.

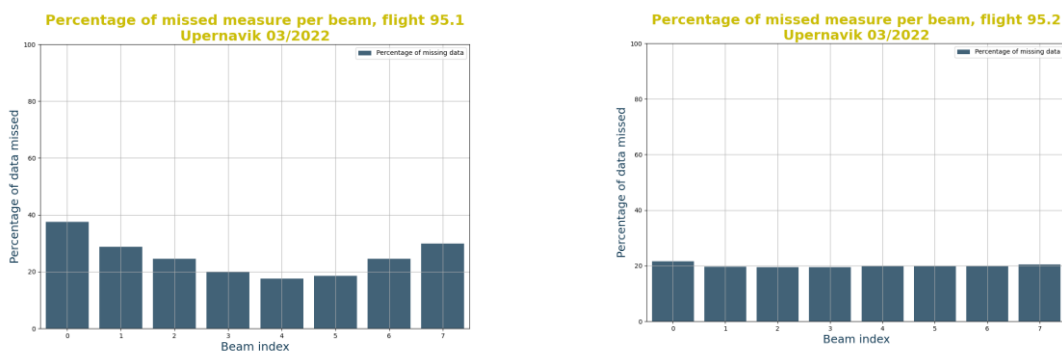


Figure 12 - Percentage of edited data for the two other LiDAR acquisitions performed on the first deployment day

Ref	NOV-FE-0899-NT-102		
Issue	2	Date	03/04/23
Rev	1	Date	17/04/23
Page	16/55		

3.1.3.2. Second day of measurement on March 30, 2022

The LiDAR acquisitions performed on the second day presents a very low level of edited data, which demonstrates the good behaviour of the LiDAR altimeter above sea ice, with a high level of backscattered signals. The percentage of edited data per LiDAR beams for the second day is presented in Figure 13.

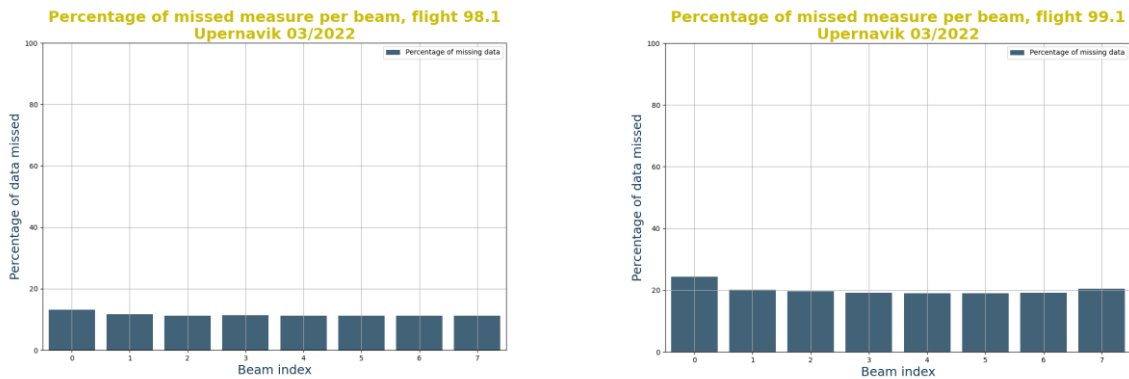


Figure 13 - Percentage of edited data of the LiDAR acquisitions performed on the second deployment day

3.1.3.3. Conclusions about LiDAR capability to retrieve measurements over sea ice

The LiDAR acquisitions show excellent performances in terms of percentage of edited data over sea ice. The LiDAR back-scattered signal is very clean. The percentage of edited data on the central beams is comparable to the one obtained during hydro flights over rivers or ocean. The percentage of edited data on the exterior beams is better than the one obtained on hydro flights over rivers because the sea ice surface is very rough. Both drone and altimeter are working very well in cold conditions (temperatures down to about -13°C and wind). The GNSS positioning of the base and the altimeter is good even at these high latitudes with a challenging satellite constellation geometry compared to flights performed at lower latitudes.

The vortex.io LiDAR altimeter is working properly in Arctic conditions and is valid to measure sea ice surfaces.

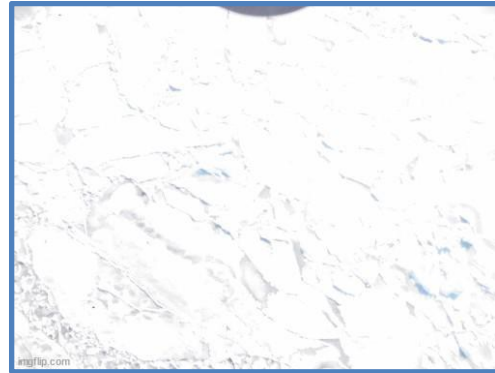
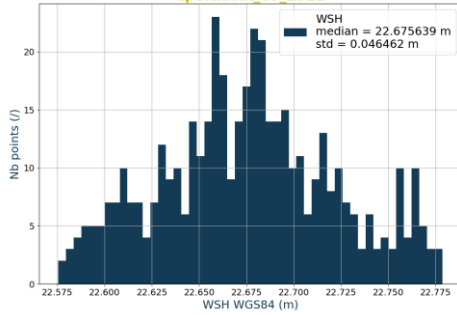
3.1.4. Sea ice surface analysis

3.1.4.1. Elevation measurements

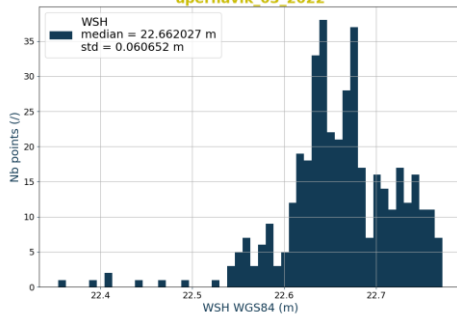
Various sea ice surfaces have been observed and measured with the LiDAR altimeter all along the different drone flights. Figure 14 presents the different elevation measurements performed by the LiDAR altimeter during the different drone flights. The elevation measurements are presented as histograms. We observed a very good precision with a standard deviation varying as a function of the surface roughness with values between 2.04 cm and 6 cm. The images allow to highlight the different sea ice type overflown during the different drone flights. We can clearly observe the different variety of sea ice surface measured in the area. These results demonstrate the value added of having pictures of the measured surface which allow us to better understand what is measured.

Ref	NOV-FE-0899-NT-102		
Issue	2	Date	03/04/23
Rev	1	Date	17/04/23
Page	17/55		

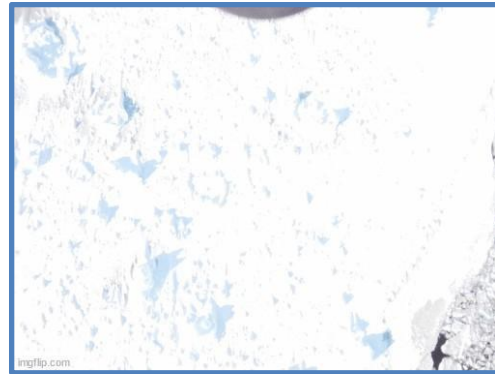
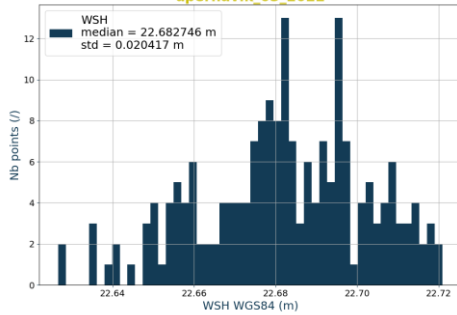
WSH measured by vortexX.io VTX-1 Flight 95.1 roughness 1
upernavik_03_2022



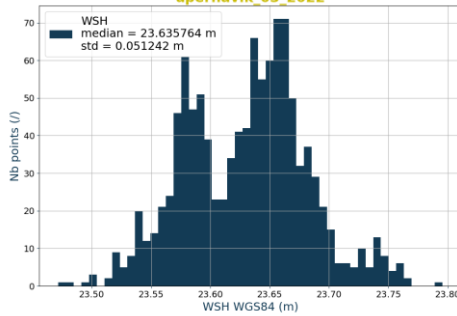
WSH measured by vortexX.io VTX-1 Flight 95.1 roughness 2
upernavik_03_2022



WSH measured by vortexX.io VTX-1 Flight 95.2 roughness 2
upernavik_03_2022



WSH measured by vortexX.io VTX-1 Flight 98.1 roughness 1
upernavik_03_2022



Ref	NOV-FE-0899-NT-102		
Issue	2	Date	03/04/23
Rev	1	Date	17/04/23
Page	18/55		

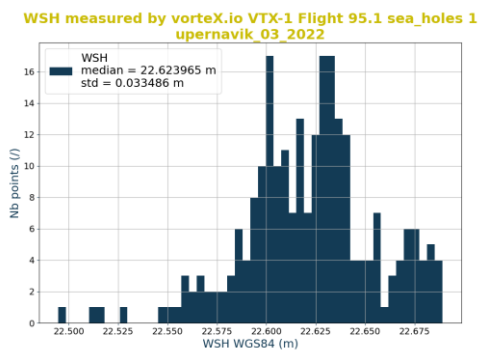
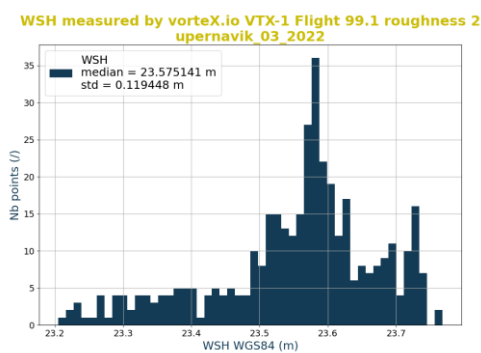
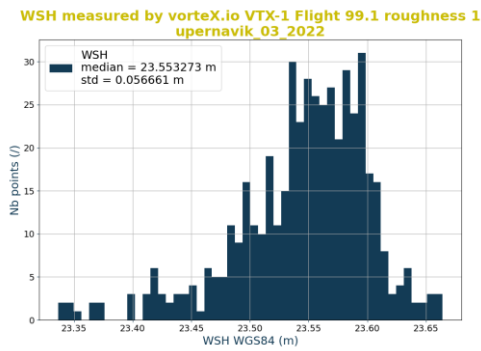


Figure 14 - Histograms of elevation measurements performed by the LiDAR altimeter over sea ice when the drone is moving (left column). Images taken by the embedded camera during the corresponding flights (right column).

Static flights have also been performed during the campaign and similar results were obtained as shown in Figure 15. The observed standard deviation ranges between 2.2 cm and 5.3 cm which is similar to the value obtained when the drone is moving. These results demonstrate that the standard deviation of elevation measurements is directly due to the surface roughness and not to the displacement of the drone during the flight.

Ref	NOV-FE-0899-NT-102		
Issue	2	Date	03/04/23
Rev	1	Date	17/04/23
Page	19/55		

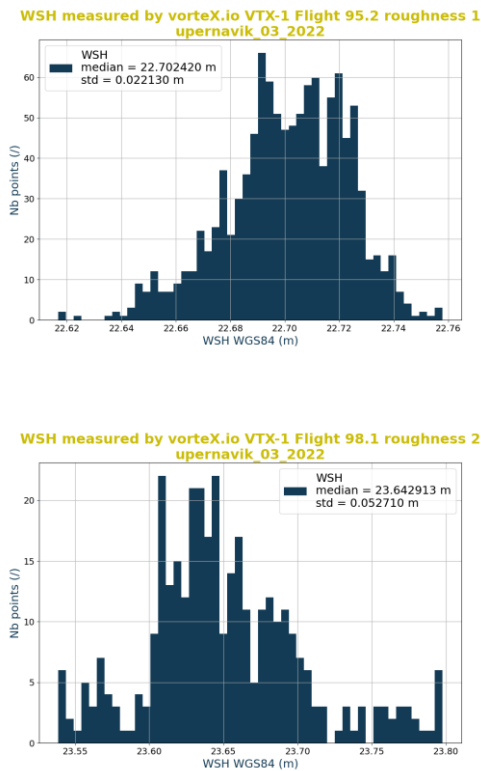


Figure 15 - Histograms of elevation measurements performed by the LiDAR altimeter over sea ice during static flights (left column). Images taken by the embedded camera during the corresponding flights (right column).

3.1.4.2. Building orthophoto of the observed surface

As the vortex.io LiDAR altimeter directly embarks a camera on-board, a picture is taken each second during the drone flight. With specific flight plans programmed on the drone (see the campaign log part), it is possible to build orthophotos of the overflow area. Orthophotos or orthoimages are geometrically rectified and radiometrically equalized images of the surface. These images, which are in the form of tiles covering an area of the Earth, are georeferenced. They can be used as background maps in Geographic Information Systems or for other usages, such as the surface classification. Figure 16 presents the results of the orthophoto built from the different images taken during the specific drone flights performed at an altitude of 100 m above the surface.

The sea ice surface is monochromic with fortunately few structures that help the algorithm to merge the pictures taken by the altimeter. The orthophoto is clear around the leads but is empty where the sea ice surface is too smooth. During this day of measurement, the luminosity was very bright, and the pictures are sometimes overexposed. Some artefacts can be observed on the orthophoto due to the lack of visible structure on the pictures but also due to the sea ice drift. Even if some discontinuities appear on the orthophoto due to sea ice drift, we can observe a lot of details. And this orthophoto can be used for applying surface classification algorithms.

Ref	NOV-FE-0899-NT-102		
Issue	2	Date	03/04/23
Rev	1	Date	17/04/23
Page	20/55		



Figure 16 - Orthophoto computed from all the images taken during specific orthophoto flights

3.1.4.3. Surface classification

Thanks to the computed orthophoto and based on simple algorithms, it is possible to compute surface classification masks. Here we used classical algorithms called NDWI for Normalised Difference Water Index. The NDWI method is an index for delineating and monitoring changes in surface water content. This index is calculated with the NIR and green channels as the on-board camera does not have an IR filter, NIR signals are collected into the red band of the camera. In this frame, we can easily compute the NDWI using the following formula:

$$NDWI = (Green - NIR) / (Green + NIR)$$

Assuming that the NIR band is equivalent to the Red band with our sensor, the obtained NDWI map is displayed in Figure 17. Thanks to the index, it is easy to compute a surface classification by applying a threshold on the NDWI value (for example $NDWI \geq 0.99$ is a sea ice surface, $NDWI < 0.99$ is a water surface).

Ref	NOV-FE-0899-NT-102		
Issue	2	Date	03/04/23
Rev	1	Date	17/04/23
Page	21/55		

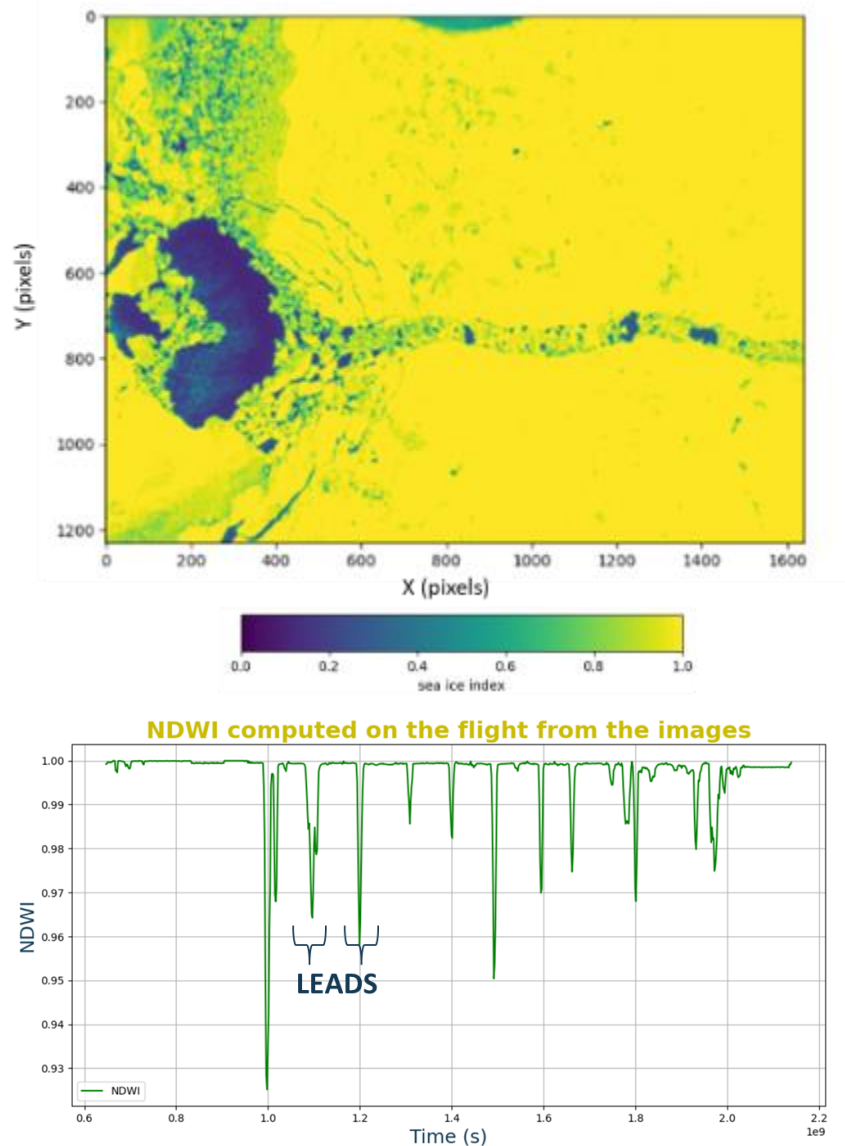


Figure 17 - Map of the NDWI computed from a part of the orthophoto (top image). Cut of the NDWI performed in the NDWI map (bottom).

3.1.4.4. Freeboard computation

During this drone campaign, small leads have been overflowed by the drone that are apparently mainly due to passages of small boats. The orthophotos allowed us to determine the width of the observed leads as shown in Figure 18. On this figure, the observed lead is 4.6 m wide. All the small leads overflowed during the campaign have a similar width with a lot of floating ice, as shown in the picture. In this context, it is very difficult to compute freeboard since no clear elevation difference is visible in the LiDAR data.

One solution is to find bigger leads or to compute freeboard at the interface between free water and sea ice. Since no bigger leads have been found in this area, the second solution has been chosen. The images displayed in Figure 19 show the measured interface.

Ref	NOV-FE-0899-NT-102		
Issue	2	Date	03/04/23
Rev	1	Date	17/04/23
Page	22/55		

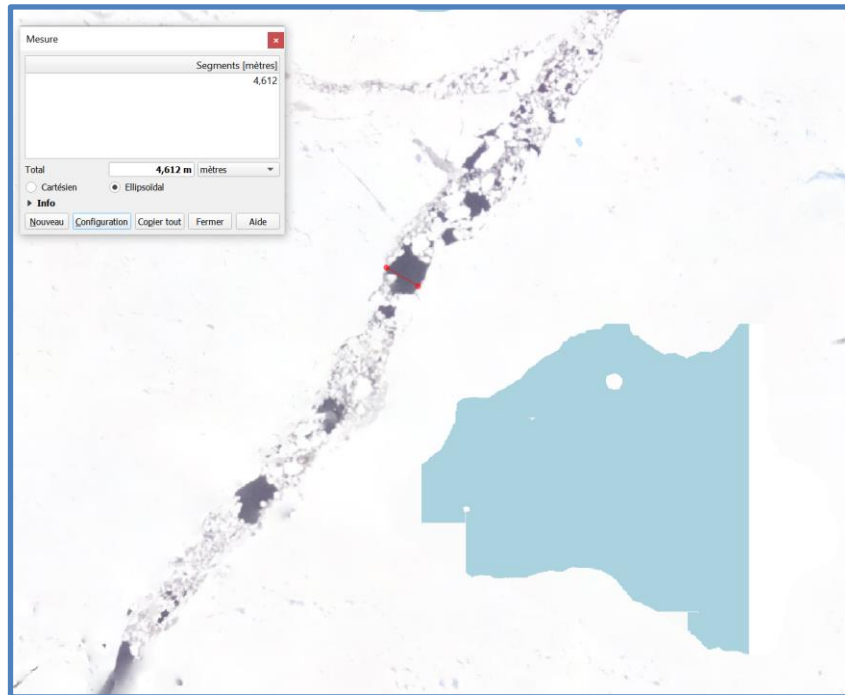


Figure 18 - Zoom on a sea ice lead in the computed orthophoto. The width of the observed lead is 4.6 m.

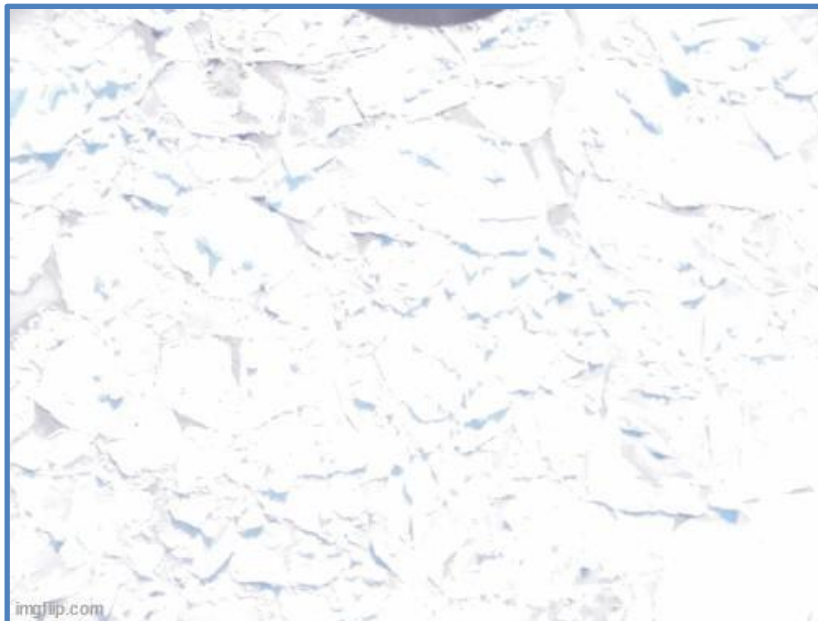


Figure 19 -Image taken by the altimeter during the overflight of the interface between sea ice and free water

By overflying the interface between sea ice and free water, it becomes possible to compute freeboard. Figure 20 shows the elevation histogram when overflying the interface between sea ice and free water. 2 different elevation distributions are clearly visible and correspond to the water surface elevation and the sea ice elevation. It is thus possible to compute freeboard from these 2 distributions. The computed freeboard is about 8 cm which is fully in line with the expectation in this region and at this time of the year. With this result we have demonstrated the capability of the vortex.io drone embedded LiDAR altimeter to measure sea ice freeboard.

Ref	NOV-FE-0899-NT-102		
Issue	2	Date	03/04/23
Rev	1	Date	17/04/23
Page	23/55		

WSH measured by vortex.io VTX-1 Flight 95.1 free_water 1
upernavik_03_2022

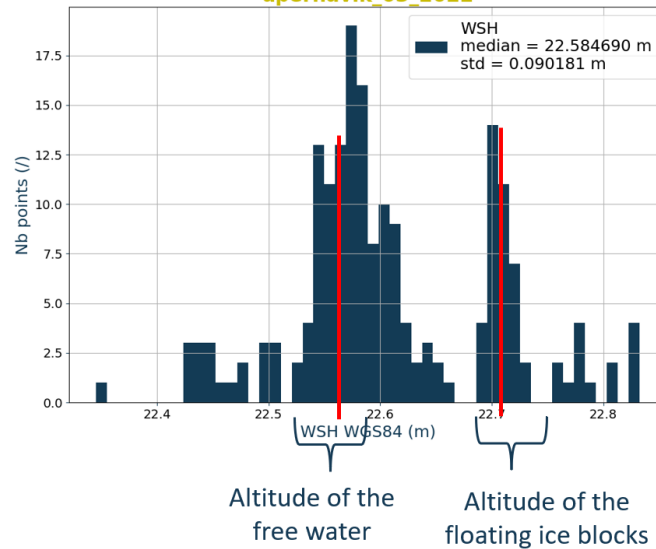


Figure 20 - Freeboard computation at the sea ice / free water interface.

3.1.5. Conclusion of the drone campaign

Although the weather conditions encountered during the campaign did not allow us to deploy the drone at the planned location under the Sentinel-3 track, a lot of results have been obtained during this deployment.

We demonstrated the capability of the drone system and of the vortex.io LiDAR altimeter to be deployed in Arctic conditions with temperatures down to -13°C . We validated the capability to compute a precise GNSS positioning required by the drone measurements. We have validated the capability of the LiDAR to work properly over sea ice and to record valuable and accurate measurements. We demonstrated the value added of the embedded camera to take pictures of the observed surface.

An orthophoto has been computed even if some artefacts remain due to the sea ice drift, resulting in discontinuities of the observed leads. A surface classification has been computed from the orthophoto and the georeferenced images. And even if the orthophoto cannot be fully exploited, individual georeferenced images could be used to compute surface classification all along the drone flight.

Finally, we demonstrated the capability of the LiDAR altimeter to compute total freeboard at the interface between sea ice and open water.

Unfortunately, as we were not able to deploy the drone under the targeted Sentinel-3 track, we have no external data to compare to the drone measurements to validate it or to evaluate the capability of the drone measurements to be compared to Sentinel-3 measurements.

Based on all these very encouraging results, we look for future deployments of such a solution in the Arctic to improve the different processing developed in this project and to work towards an operational drone solution for Cal/Val activities over sea ice.

SENTINEL-3 TOPOGRAPHY MISSION ASSESSMENT THROUGH REFERENCE TECHNIQUES (ST3TART)	Ref	NOV-FE-0899-NT-102		
	Issue	2	Date	03/04/23
	Rev	1	Date	17/04/23
	Page	24/55		

3.2. Ice-T Buoy (LOCEAN)

Snow is a major source of error for satellite altimetry and is thus part of the parameters that need to be measured in situ as accurately as possible along with sea ice thickness and freeboard for satellite data validation (so called FRM).

Technological developments were carried out in 2021-2022 to enhance snow measurement capabilities of the Ice-T buoy, with the integration of a pair of miniature FMCW radars operating at 120 GHz and 24 GHz, respectively.

Prior to their operational deployment in Baffin Bay in April 2022, a technical test was carried out in the French Pyrenees mountains early February 2022 (Figure 21) in order to:

- 1) assess snow penetrating capabilities of the radars
- 2) find the most appropriate incidence angle to guide mechanical implementation
- 3) test the various modes of each FMCW radar (e.g., bandwidth swept by the chirp that controls the resolution) to finalize software implementation.



Figure 21 - Experimental set up for testing the snow radars at different incidences (Col d'Azet, French Pyrénées, 7 February 2022)

It turned out from these tests that the 24 GHz radar returned an echo shifted by 10-15 cm with respect to the snow surface: it is not clear whether such a shift is merely a measurement bias or reflects an (incomplete) penetration of the snow. The 120 GHz radar, focused by a lens, appeared much more promising. The snow surface was accurately detected, in particular at normal incidence. The accuracy was degraded at incidences larger than 30° (Figure 22). Additional tests performed by inserting a metal sheet at the base of the snow (aimed at mimicking a conductive sea-ice layer) showed that it is possible to detect the snow base as a secondary echo, at normal incidence, even at 120 GHz, which came as a surprise given the greater attenuation at higher frequency.

Ref	NOV-FE-0899-NT-102		
Issue	2	Date	03/04/23
Rev	1	Date	17/04/23
Page	25/55		

site: Azet - Radar 122S

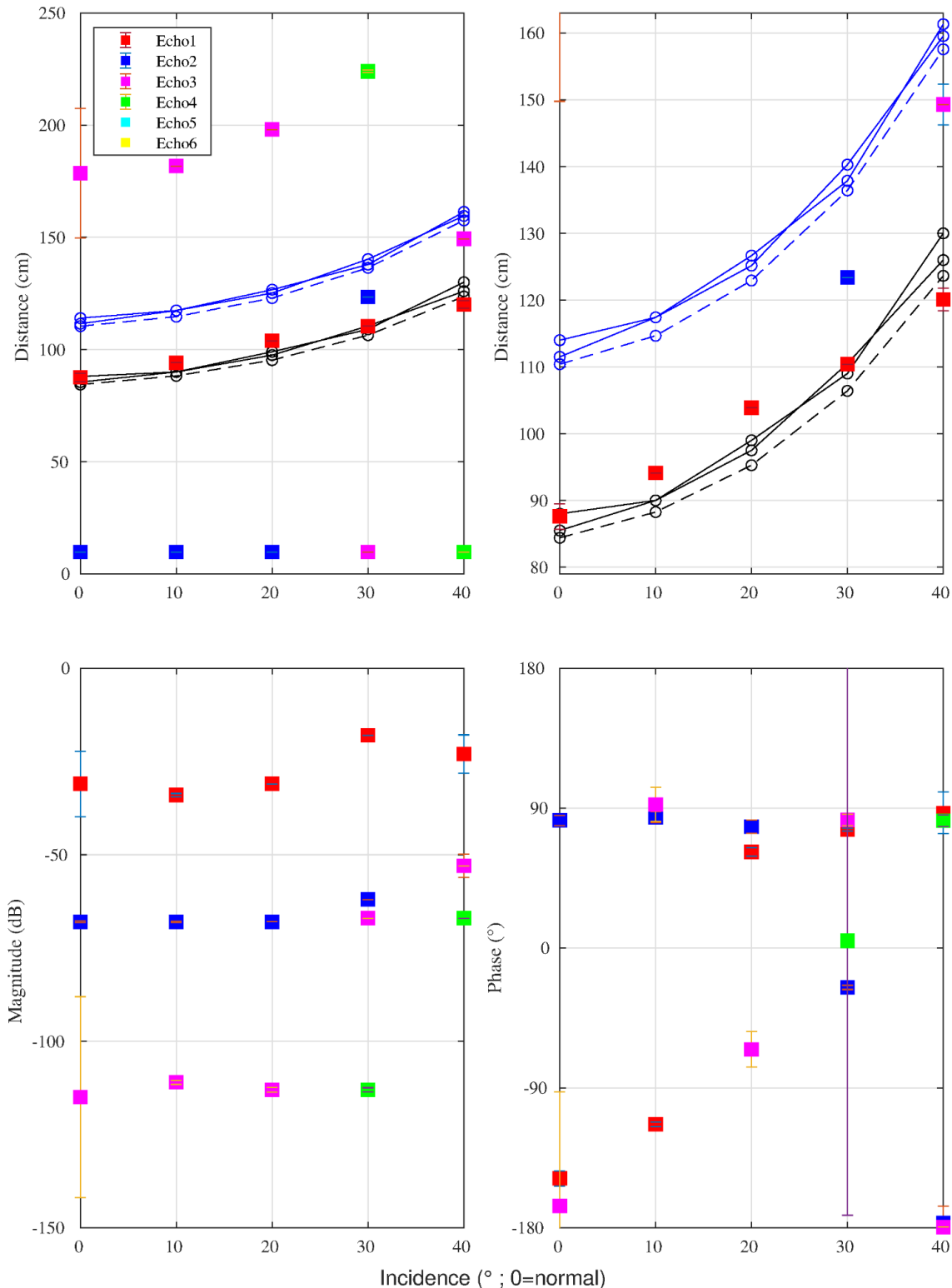


Figure 22 - Synthesis of tests at Col d'Azet for the 120 GHz radar operating in standard acquisition mode for various incidence angles. Squares denote the median of the subset of data frames for each echo/target and the error bar denotes the standard deviation over the subset of frames. For top plots the solid black line denotes the measured distance between the radar and the target point at the snow surface while the blue line is the distance to the target on the ground at the base of the snow (the dashed line is the computed distance assuming a flat surface)

Ref	NOV-FE-0899-NT-102		
Issue	2	Date	03/04/23
Rev	1	Date	17/04/23
Page	26/55		

The conclusion of these tests was that it should be possible to detect both interfaces of the snow layer (surface and base) with good accuracy provided these are operated at near normal incidence. The data collected during the tests were also crucial to develop the real-time data processing/reduction methodology since only a limited amount of information can be transmitted through the iridium satellite communication system. The full integration of the two radars on the buoy were completed in time for a first operational deployment late March 2022 in Baffin Bay as a component of the ST3TART sea-ice validation experimental setup. The mechanical design is shown in Figure 23.



Figure 23 - Ice-T buoy with 120 GHz and 24 GHz snow radars mounted on top. Deployment in Baffin Bay offshore Upernavik, Greenland, on 31 March 2022 in 55 cm-thick sea ice underneath a Sentinel 3 ground-track.

The buoy was deployed underneath a Sentinel 3B ground-track (cycle 64, absolute rev. # 20464) in a thin (55 cm) sea ice floe on March 31 2022 (Figure 23). Ancillary in-situ data include manual ice and snow depth measurements, snow density measurements and the collection of an ice core for the determination of a profile of sea ice density and salinity. The different sensors of the buoy worked perfectly. In particular, snow radars provided the expected measurements. Unfortunately, data transmissions from the buoy ceased abruptly after two weeks for an unknown reason. There is no element whatsoever that would lead to suspect an issue with the electronics or software of the buoy (all received parameters were nominal until the last iridium message). As well, inclinometer data shows the absence of change in the tilt of the ice flow so that the hypothesis of a destruction by a compression crest is unlikely. The most likely hypothesis is that damage was caused to the buoy (or at least to its antenna) by a polar bear. Polar bears were indeed very present in the area given the thin sea ice conditions with ubiquitous open water zones (leads); polar bear foot tracks were actually observed during the deployment field work. We provide below further details on the collected data set.

The buoy initially drifted southwestward before veering south to southeast, stopping transmissions on April 14 (Figure 24). Water temperature and salinity measurements collected by the buoy 6 m below the ice base indicate that the temperature always exceeded the fusion temperature of the ice, sometimes by more than 0.5°C, thus promoting basal ice melt (Figure 25).

Ref	NOV-FE-0899-NT-102		
Issue	2	Date	03/04/23
Rev	1	Date	17/04/23
Page	27/55		

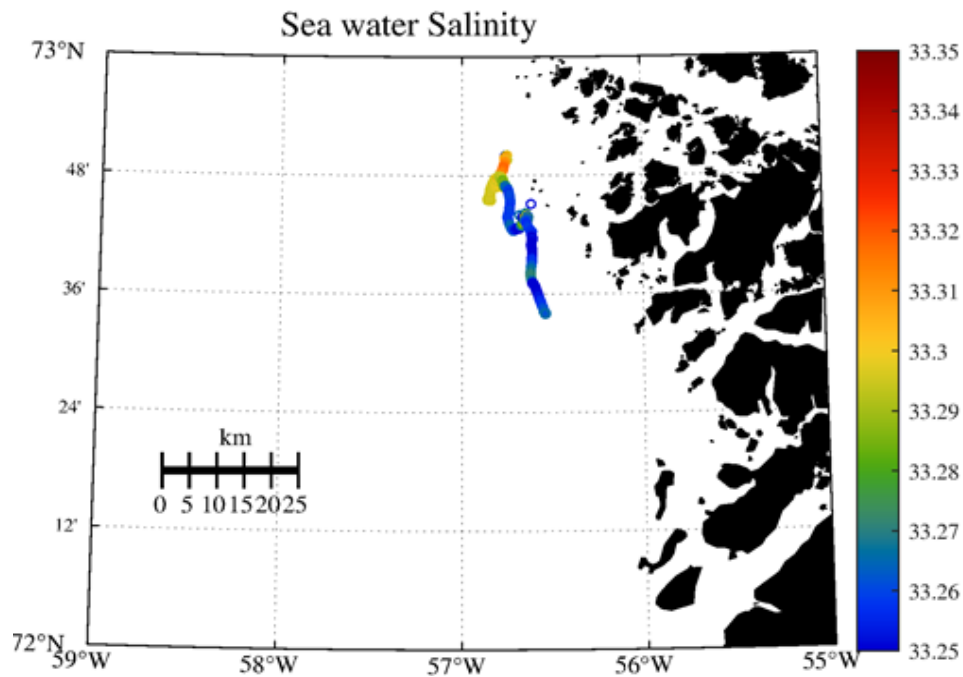


Figure 24 -Sea water salinity 6m below the sea ice measured every 15 minutes along the drift of the Ice-T buoy between March 31 and April 14 2022.

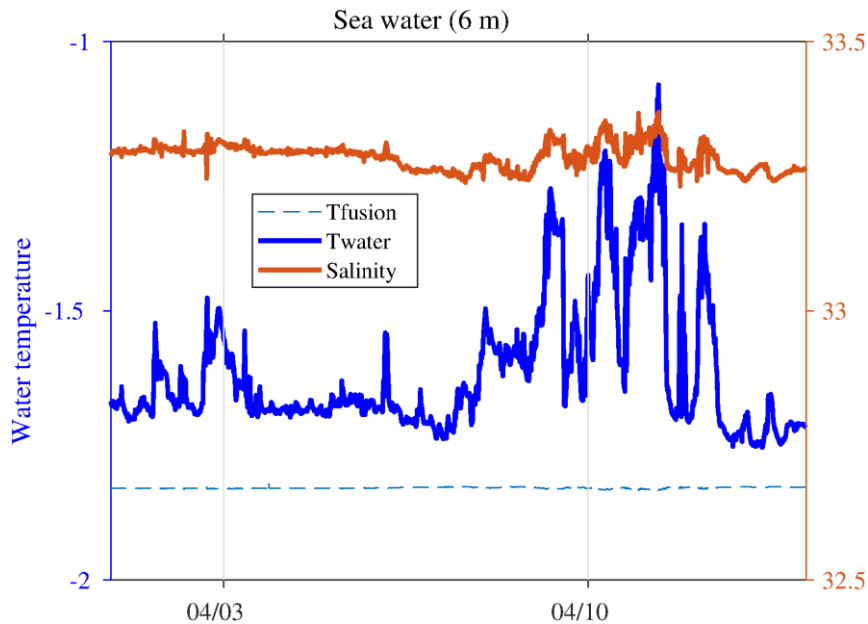


Figure 25 -Water salinity (red, scale to the right) and temperature (blue) 6m below the ice. The fusion temperature computed from in situ salinity is indicated (blue dashed line).

3.2.1. Sea ice thickness

A 56 cm long ice core was taken next to the buoy at the time of deployment (Figure 26). The short time on the sea ice did not enable to realize a long “snow line”, and manual soundings were only performed within a few meters around the buoy, yielding a snow depth on the order of 6 cm. Snow density was measured on site in collaboration with DTU (350 kg/m³). The ice core was processed as soon as possible back in Upernavik; it was divided in 10 cm segments, the density of which was measured to provide a vertical profile (Figure 27). The average ice density was 910 kg/m³. Ice samples were then melted for subsequent salinity measurement back at the lab. The bulk salinity was 6 psu or larger, with a marked saltier layer (12 psu) near the surface (Figure 27, right).

Ref	NOV-FE-0899-NT-102		
Issue	2	Date	03/04/23
Rev	1	Date	17/04/23
Page	28/55		



Figure 26 - 56 cm ice core collected close to the buoy during deployment on March 31, 2022

Ref	NOV-FE-0899-NT-102		
Issue	2	Date	03/04/23
Rev	1	Date	17/04/23
Page	29/55		

Ice Core 56 cm (31/03/22 12h30LT)

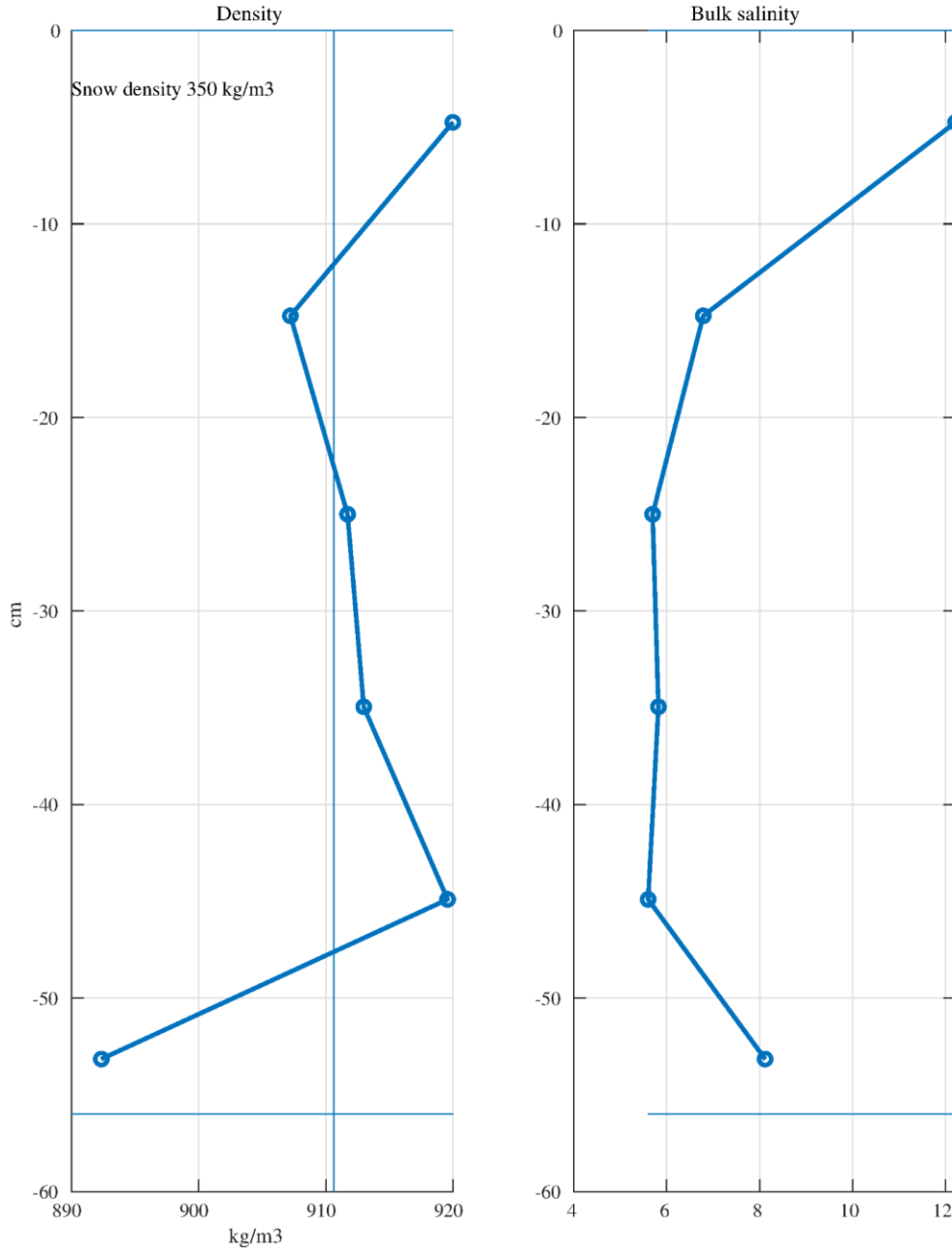


Figure 27 - Profiles of density (left) and bulk salinity (right) obtained from the ice core.

The evolution of ice thickness and freeboard as measured by the Ice-T buoy is provided in Figure 28 and Figure 29, respectively. The thickness decreased by a few centimetres over the two weeks. This melting is consistent with the water temperature exceeding the fusion point of the ice (Figure 25).

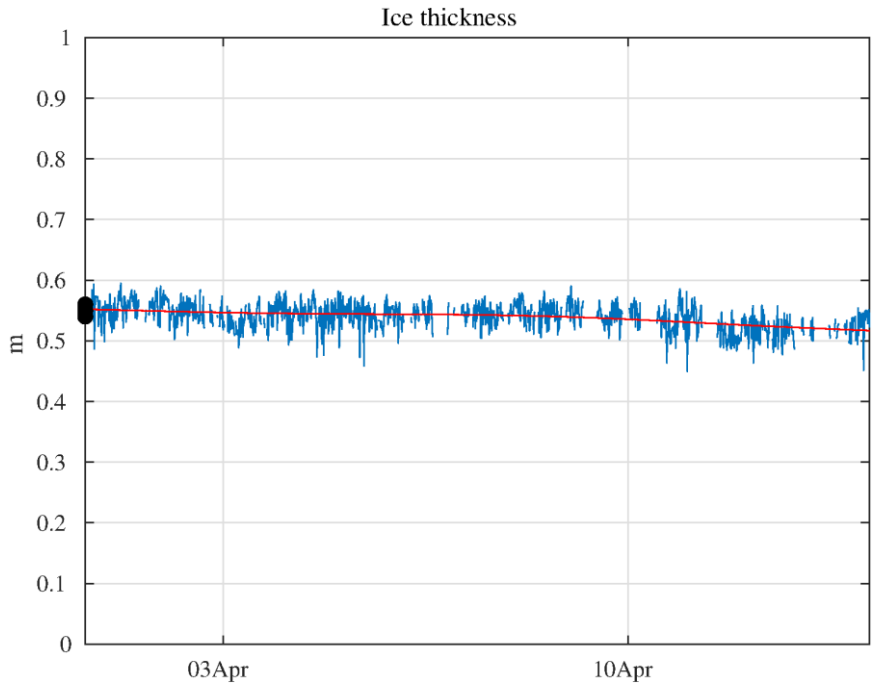


Figure 28 - Ice thickness from the Ice-T buoy (raw measurement in blue, low pass filtered in red). Black dots indicated manual soundings around the buoy at the time of deployment.

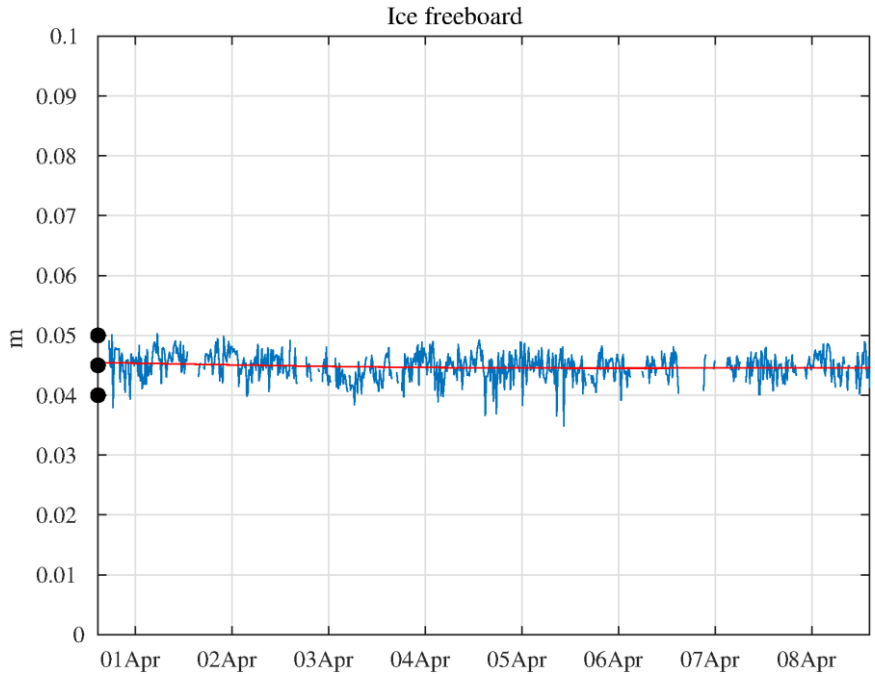


Figure 29 - Ice freeboard from the Ice-T buoy (raw measurement in blue, low pass filtered in red). Black dots indicated manual freeboard measurements around the buoy at the time of deployment.

SENTINEL-3 TOPOGRAPHY MISSION ASSESSMENT THROUGH REFERENCE TECHNIQUES (ST3TART)	Ref	NOV-FE-0899-NT-102		
	Issue	2	Date	03/04/23
	Rev	1	Date	17/04/23
	Page	31/55		

3.2.2. Snow experiment

Both FMCW snow radars were alternatively operated in two modes: Low Resolution (LR) and High Resolution (HR), with a larger chirp bandwidth. The 24 GHz radar did work but returned only the snow surface echo. The 120 GHz beam was focused with a lens and returned consistently the snow surface echo (Figure 30), but also (not systematic) a secondary echo corresponding to the ice surface, and even a third weak echo that seems to correspond to the ice base, provided a correction for the EM waves celerity in the ice is made (a factor ~ 0.6 in dry ice at 120 GHz). The data are therefore very encouraging with respect to the objectives. In HR mode, the snow surface is tracked with a few-millimetre resolution, but additional filtering is needed (Figure 30, middle). The interest of the LR mode is for the disambiguation of multiple echoes. There has been significant variability during the record. At least one snowfall occurred at the beginning (documented), consistent with the diminution of the measured distance after deployment. The surface temperature record from the buoy suggests multiple thawing-freezing cycles.

Ref	NOV-FE-0899-NT-102		
Issue	2	Date	03/04/23
Rev	1	Date	17/04/23
Page	32/55		

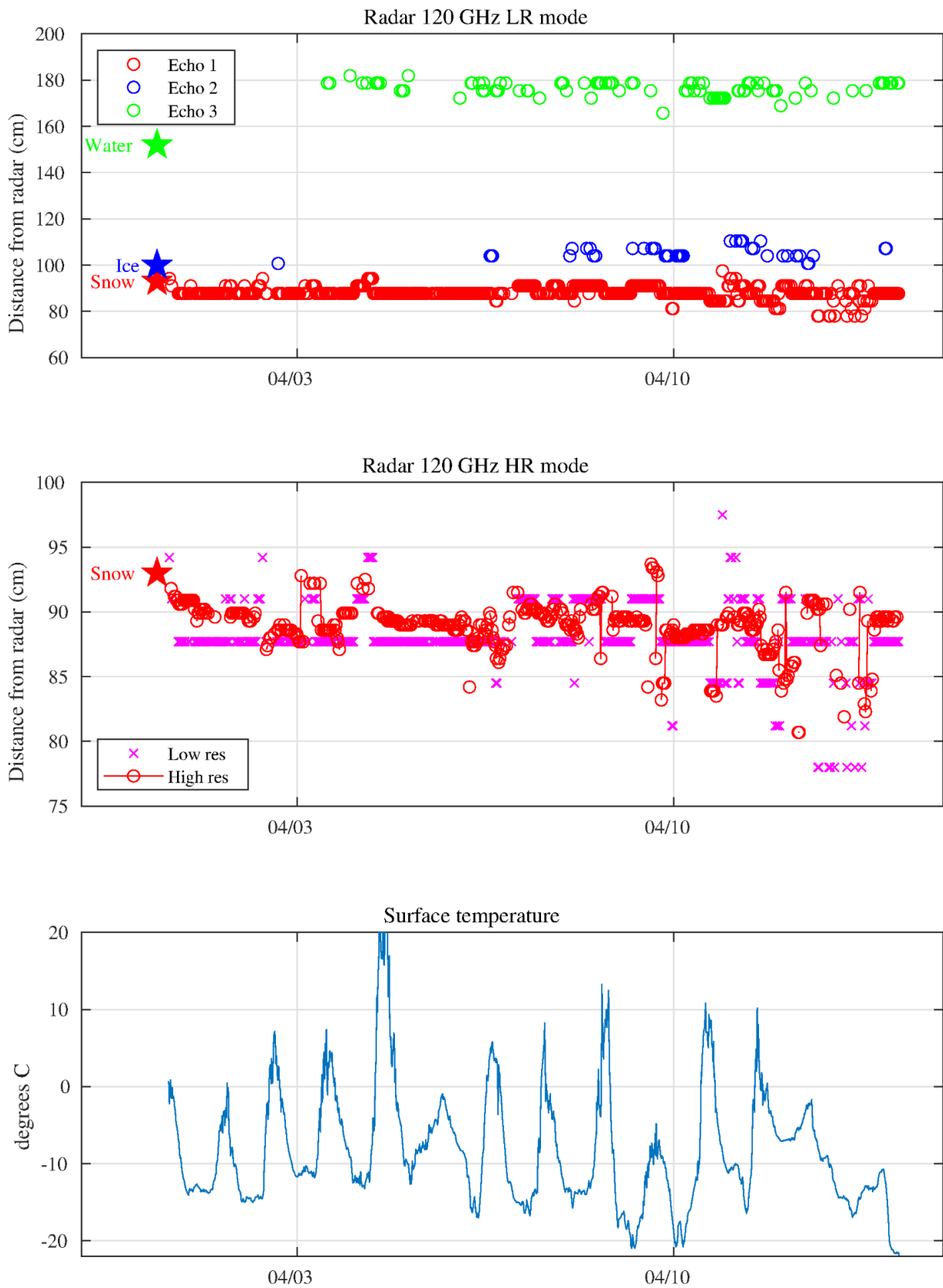


Figure 30 - Distance to the target measured by the 120 GHz radar in LR mode (top) and HR mode (middle). Stars at the beginning of the series indicate distances to the different targets measured on the field during deployment. The evolution of the air temperature as measured by the buoy is indicated (bottom).

Ref	NOV-FE-0899-NT-102		
Issue	2	Date	03/04/23
Rev	1	Date	17/04/23
Page	33/55		

Subsequent analyses are aimed at evaluating if the snow depth record is consistent with other data sources. The only available option at the moment is to compare with atmospheric model outputs (ERA5 reanalysis). Before focusing on snow depth, as an initial ERA5 assessment, we examine whether ERA5 air temperature and atmospheric pressure interpolated along the buoys trajectory are consistent with the buoy's measurements. ERA 5 air temperature (2m) is smoother and biased low compared with Ice-T shelter temperature, measured under the buoy's hat (Figure 31, left). Temperature measurements along the buoy, which are exposed to solar radiation, suggest frequent snow melt episodes ($T > 0$). Likewise, ERA5 atmospheric pressure is much smoother compared with the buoy's data (Figure 31, right), with a missed storm at the beginning of the measurement period, that was associated with snow fall. The large scale, low frequency variability is otherwise relatively well captured.

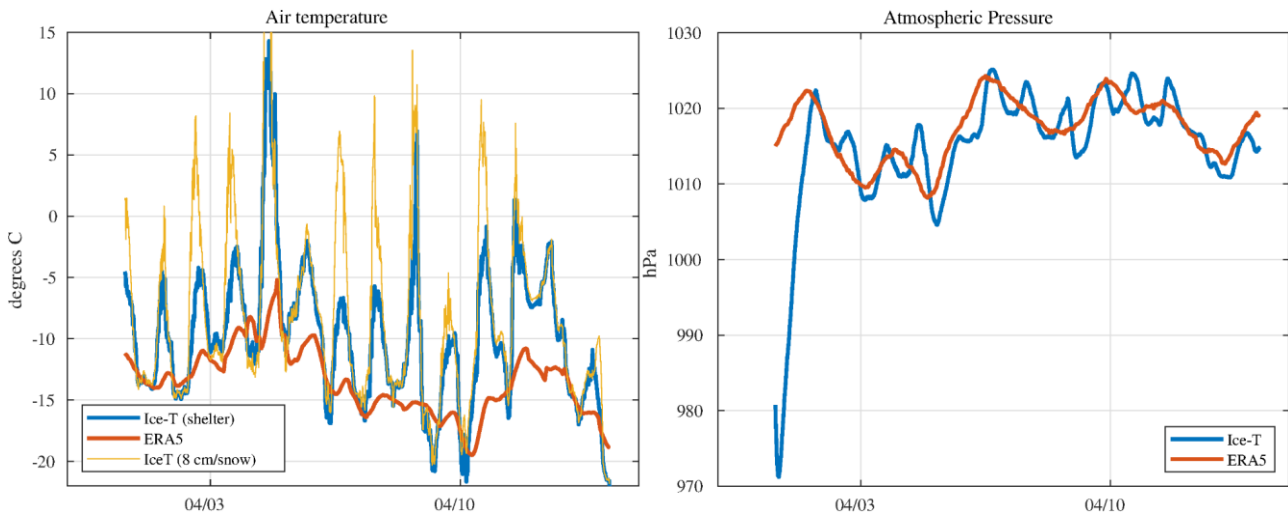


Figure 31 - Left: Comparison of ERA5 2-m air temperature (red) with the buoy's data under its hat (shelter temperature, blue) and along the buoy 8 cm above the snow surface (yellow). Right: comparison of ERA5 and Ice-T atmospheric pressure data.

Regarding snow, two parameters are available from ERA 5: snowfall and snow depth. The latter is the result from snow fall, settlement and melting. Both parameters have been interpolated along the buoy's trajectory (Figure 32). Accumulated snowfall (starting from 0) is shown rather than snow fall (its time derivative). These parameters are provided in terms of water height equivalent in ERA5 and thus need to be divided by the snow density for comparison. The snow density used in ERA5 is 100 kg/m^3 , which is much smaller than the 350 kg/m^3 measured on site on March 31. Both values are shown in the Figure 32.

ERA 5 snow depth interpolated along the buoys trajectory does not look right. From zero it sharply rises to 18 cm (for a density of 100 kg/m^3): its variations are inconsistent with ERA5 collocated snowfall evolution (Figure 32). Snow depth may not be relevant above sea ice, at least above thin ice, owing to the heterogeneous sea ice cover (ice concentration < 1), which is furthermore drifting, making it very difficult for the model to keep track of the snow cover evolution. Accumulating ERA5 snowfall appears to provide a more realistic information, at least to get an idea of the timing and intensity of precipitation (snow settlement, snow melt is not included; issue with snow density). How realistic is this estimate though? We see for instance that the initial snowfall (that we did observe) was not captured (the corresponding storm was not captured in atmospheric pressure data). This suggests that it may at best be taken as a rough guidance.

Ref	NOV-FE-0899-NT-102		
Issue	2	Date	03/04/23
Rev	1	Date	17/04/23
Page	34/55		

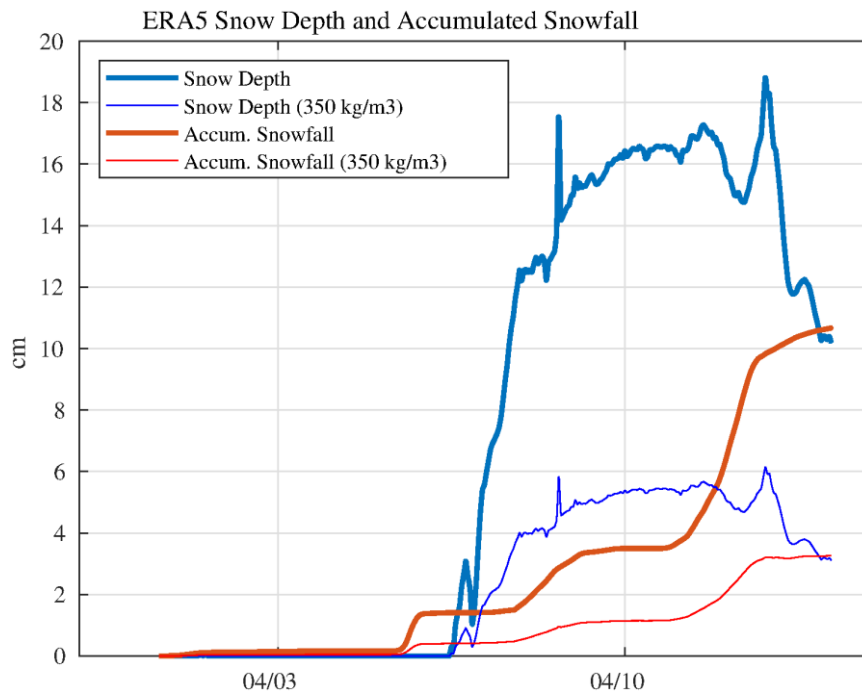


Figure 32 - ERA5 Snow Depth and Accumulated Snowfall (starting from 0) interpolated along the buoy's trajectory. Two values of snow density are used for the conversion: 100 kg/m³ (ERA5 value) and 350 kg/m³ (value measured on site during deployment).

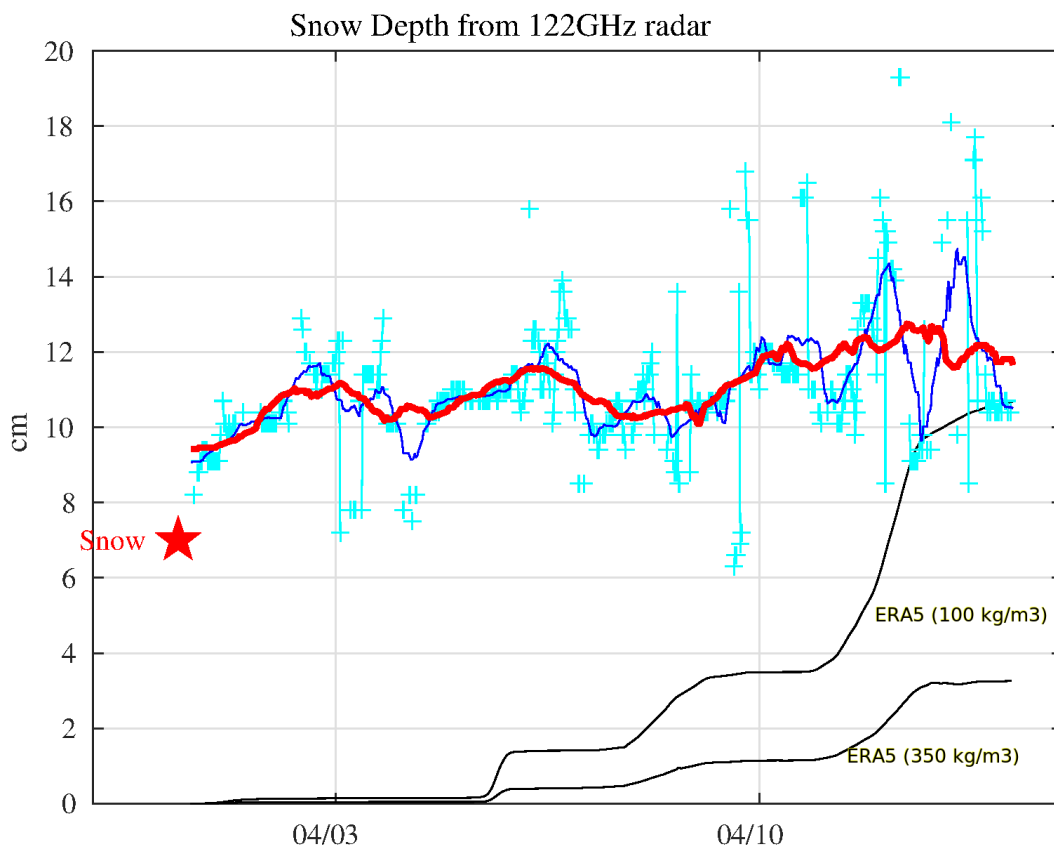


Figure 33 - Snow depth measured by the buoy (raw data in cyan, low pass filtered in red). Accumulated snowfall from ERA 5, using two values for snow density (100 and 350 kg/m³) is shown in black.

Ref	NOV-FE-0899-NT-102		
Issue	2	Date	03/04/23
Rev	1	Date	17/04/23
Page	35/55		

The radar distances of Figure 30 have been converted to snow depth in Figure 33, where both raw values and a final estimate after low pass filtering are displayed. The general evolution is that of a small increase in snow depth over the 15-day period, on the order of 2-3 cm. This order of magnitude is consistent with the accumulated snowfall from ERA5, assuming a snow density of 350 kg/m³ as was measured on the field (bottom black line in Figure 33).

We find no correspondence with ERA 5 snowfall as far as short time scale variations are concerned, but as discussed above, ERA 5 snowfall is probably not very accurate here. What remains unclear is the episodic noise (~ 2cm RMS) in the raw data, which we did not experience during the technical tests in the Pyrénées. Intermittent snow melt and the presence of liquid water could be a hypothesis, but we did get snow melt during the technical tests, with no impact. Another, more likely, hypothesis is the influence of the wind, causing vibration in the superstructure. The superstructure holding the mast was engineered to be light (thus subject to vibration) so as to be sacrificial in case of polar bear attack, to avoid the iridium antenna used for data transmission to be damaged (a strategy that was apparently insufficient here).

Overall the buoy did provide the expected measurement. The short record was a disappointment (we expected a couple of months of data from drift simulations in the Baffin Bay), especially as all sensors were working well. The ice conditions found offshore Upernavik in the spring 2022 were similar to what is usually found in the Marginal Ice Zone, with the presence of open water and drift ice greatly increasing chances of an encounter with a polar bear. The accuracy reached here for snow depth measurements (estimated on the order of a couple of cm) will be improved after a full assessment of the origin of the reported episodic noise.

The comparison of buoy data wrt ERA5 are overall not very promising. Snow depth from combined SARAL/AltiKa and S3 or ICESat-2 and S3 freeboards can be used to compare to the snow depth miniature radars in future, when the new baseline for S3 sea ice processor has been fully implemented and validated. However, For this study the data is obtained relatively close to the coast, which can be challenging for the satellite altimetry sensors. Buoy deployment north of 81.5°N needs estimates of snow depth from combined ICESat-2 and CryoSat-2. Alternatively, sources to obtain snow depth measurements in the buoy area shall be explored prior to deployment.

3.3. Airborne data

The airborne data has been processed using standard procedures as described in TD-10-2 “TD-11-2 FRM Campaign Technical Handbook for S3 STM Sea Ice Products” Section 1.2.

3.3.1. Sea ice freeboards from lidar

The freeboards extracted from the airborne lidar is the total freeboard (ice + snow). Total freeboards from ALS along S3A and S3B orbits from flights on March 27 and 30, respectively, are shown in Figure 34. The associated total freeboard distributions are provided in the upper right corner with flights along S3A orbit in white and S3B in blue. The total freeboards are relatively low with modal values between 10-20 cm. This corresponds well with in situ measurements obtained during buoy deployment.

We can directly use the data from the Ice-T to convert total freeboard into thicknesses and thus reduce the uncertainties on the sea ice thickness estimates.

$$h_i = \frac{f_s \rho_w}{(\rho_w - \rho_i)} + \frac{h_s (\rho_s - \rho_w)}{(\rho_w - \rho_i)}$$

Ref	NOV-FE-0899-NT-102		
Issue	2	Date	03/04/23
Rev	1	Date	17/04/23
Page	36/55		

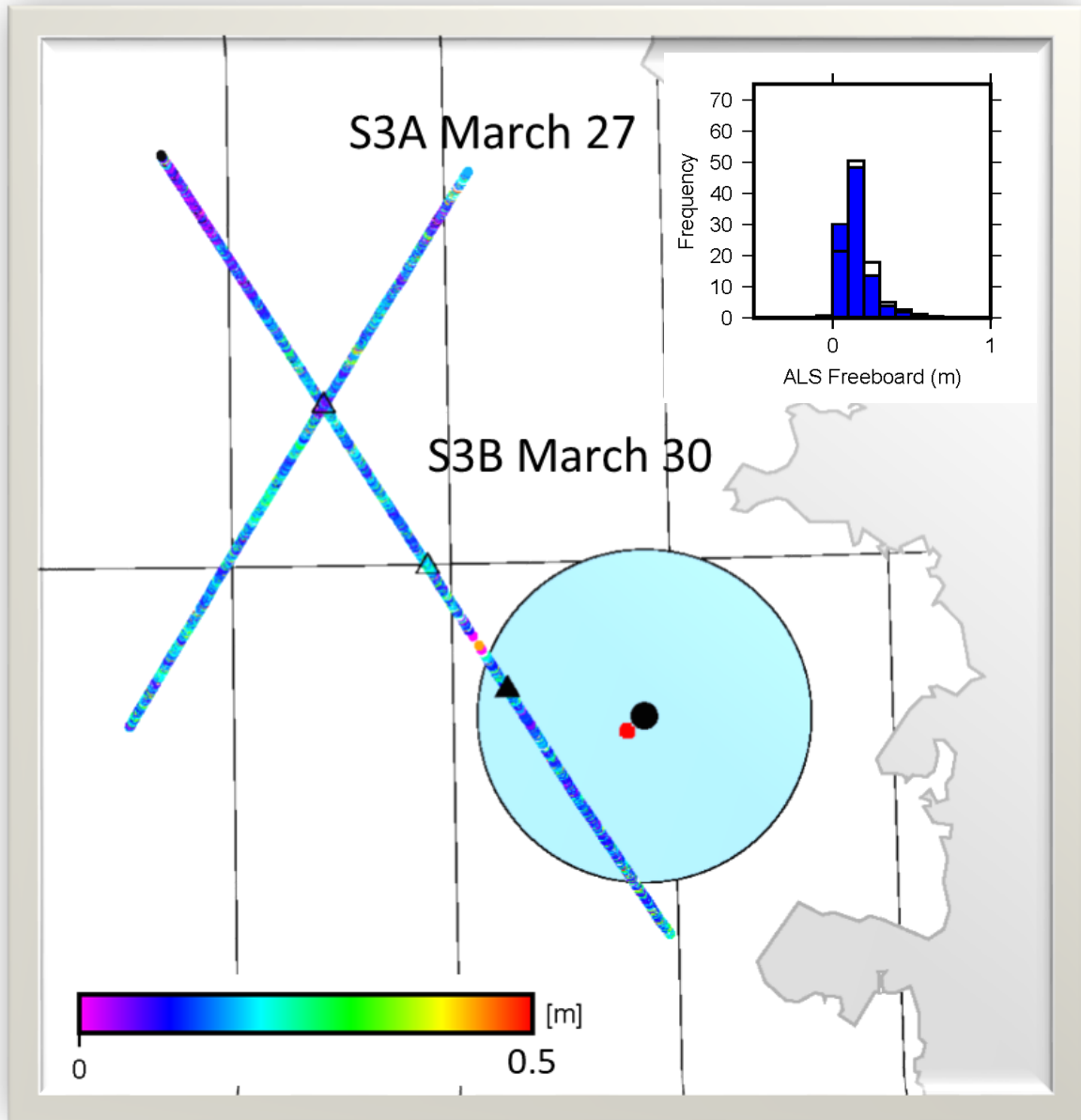


Figure 34 - Total sea ice freeboards from ALS along S3A and S3B orbits from flights on March 27 and 30, respectively. In upper right corner is the associated ALS distributions with S3A orbit in white and S3B in blue.

3.3.2. Sea ice freeboard from Ku/Ka-band radar altimeters

As this is the first time DTU is processing the radar data it takes a bit longer than usual. We are in contact with CRISIS, and we do expect to have these results ready for the Final Meeting on April 20.

3.3.3. Surface classification from visual images

To support the analysis of CReSIS and ALS data especially over sea ice, high-resolution images are collected along the flights. A nadir looking GoPro3 camera was installed on the metal plate, which also holds the four CReSIS antennas. The field of view of the camera is slightly obstructed by the antenna structure but with a sample rate of 5 sHz the images have large overlaps. Note; The older version, GoPro3, has proven to be more stable under cold conditions, therefore this has been chosen as the primary camera.

Slant looking images were obtained using a GoPro7 camera, when the GoPro3 failed during flight. The camera was mounted in the rear starboard window in the cabin. Both cameras were remotely controlled, and time tagged using the internal camera clock. By combining the time tag of the images with GNSS data the images can be geo-located along the flight lines. This is work in progress. An overview of the properties of the cameras is given in Table 1 and image examples are shown in Figure 35 and Figure 36.

For future campaigns the images should be provided as geo-tiff or similar format, to fully utilize the images for surface classification.

Table 1: Overview of camera types and settings.

Camera type	View	Interval (sec)	Resolution (pixels)	Image size (MB)	Software program	Format
GoPro 3	Nadir-looking	5	2600 x 2000	~2.0	GoPro app	JPEG
GoPro 7	Slant-looking	5	3000x4000	~2.2	GoPro app	JPEG

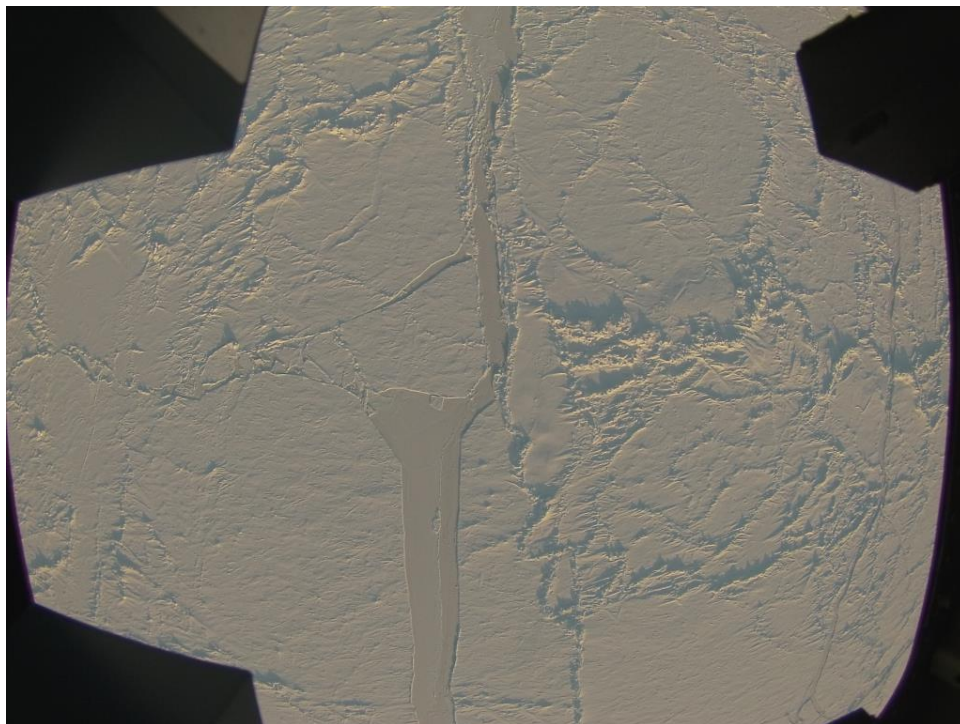


Figure 35 - Examples of nadir looking image from GoPro3 (left), April 6th

Ref	NOV-FE-0899-NT-102		
Issue	2	Date	03/04/23
Rev	1	Date	17/04/23
Page	38/55		

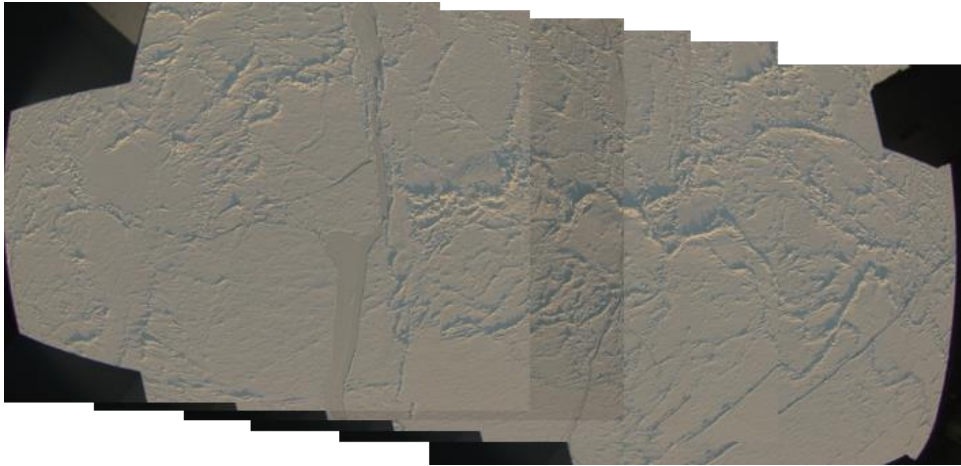


Figure 36 - Examples of nadir looking images from GoPro3 (left), April 6th; series of six photos with 5 sec intervals, showing overlap between images.

3.4. Drone from ship (LEGOS)

The motivations and the implementation of the Drone Experiment for Sea Ice Retrieval (DESIR) have been described in the log report “NOV-FE-0899-NT-103_TD12-DESIR Campaign log”. Here we present the datasets that have been collected, the methodology applied to retrieve the freeboard and the comparisons against alternative datasets.

3.4.1. Description of the datasets

The main objectives of the DESIR experiment were to determine the feasibility to measure the sea ice freeboard using a drone equipped with a lidar. We present here the lidar data that were collected, as well as the measurements that were made in the field and those obtained with the SIMS sensor at the front of the ship.

3.4.1.1. Lidar datasets

During this campaign we were able to make about 10 flights with the drone, including 3 with the YellowScan 3D scanner over the ice pack. These measurements were made on July 15 and 16, 2022. Each flight lasted about 20mn. The YellowScan acquired about 220,000 measurement points per second. Each measurement is associated with about ten parameters, including the time, the 3D position of the measurement (x,y,z) within WGS84 referential, the angle of the laser shot, the returned energy, etc. The data are stored in .LAS standard files used for point clouds. Their Zip-compressed version is identified by the .LAZ extension. For 20 minutes of flight this represents .LAZ files of about 1GB and thus 3 Go for the 3 flights. A typical scene is shown Figure 37.

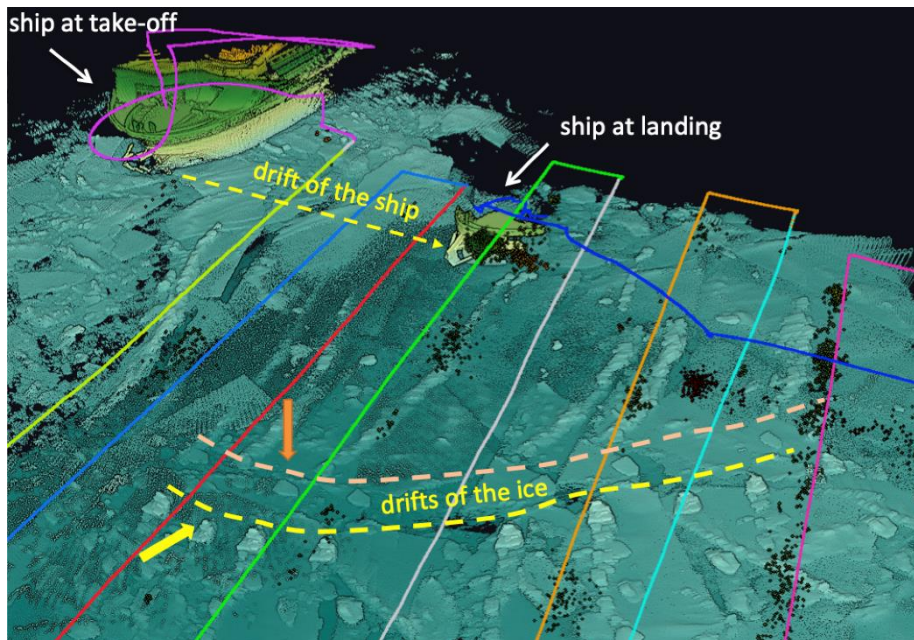


Figure 37 - A typical scene acquired with the 3D lidar scanner YellowScan during 1 flight. The colour lines represent successive paths of the drone.

As can be seen on this figure, the same floes are seen several times and at different locations along the path of the drone. This is due to the fact that the ice pack is drifting in a consistent way. Therefore it is not possible to reconstitute a 3D scene with all the measurements (see explanations developed in the TD-12 report of this mission).

Moreover, the GPS position of the drone (or, more precisely, that of the GPS integrated into the YellowScan to geolocate the measurements) is very imprecise. For example, the figure below shows a difference in height of 1.75m between the same floe perceived by 2 successive tracks. The 2 measurements are however separated by only a few tens of seconds and a few hundred meters.



Figure 38 - A section of the previous 3D scene shows in the lower part the same floe observed by 2 successive tracks of the drone. This floe is perceived as translated of 1.75m in height between these 2 observations distant only a few tens of seconds and a few hundred meters.

Ref	NOV-FE-0899-NT-102		
Issue	2	Date	03/04/23
Rev	1	Date	17/04/23
Page	40/55		

We therefore decided to process the data track by track (each colour path of Figure 37). Thus we split the 3 flight trajectories into a set of tracks and we obtained 12 tracks for the flight of July 15, 5 tracks for that of July 16 at 11 am and 22 tracks for that of July 16 at 12 am.

3.4.1.2. Sea Ice Measurement System (SIMS) datasets

The Commandant Charcot is equipped with an ElectroMagnetic (EM) sensor suspended at the front of the boat as in Figure 39 and Figure 40 illustrated below.



Figure 39 - The SIMS ElectroMagnetic sensor suspended from the front of the boat allows to real time measurements the total Sea Ice Thickness (including the snow). We can also guess the drone in front of the ship, at the level of the SIMS support beam.

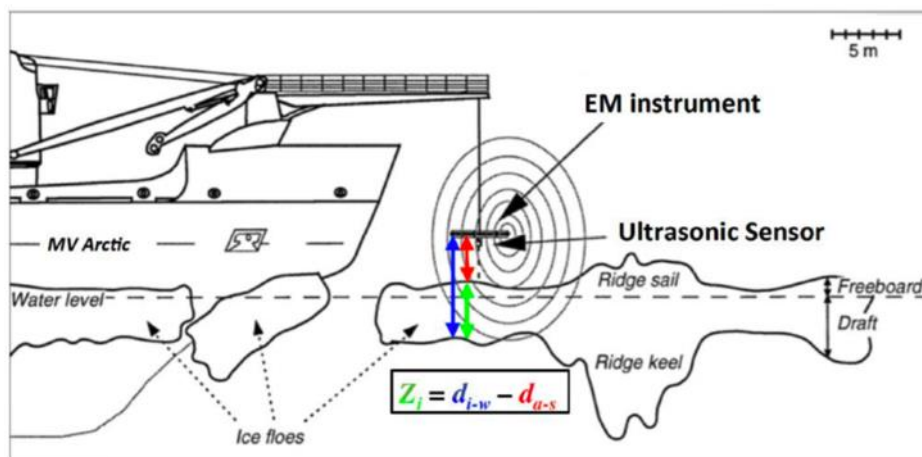


Figure 40 - SIMS measurement principle.

The SIMS acquires data every second. This data is retrieved by the ship's command bridge in real time and stored in CSV format files. The SIMS is continuously activated while the ship is navigating through the ice. We thus have data from July 9 to 18. For an unknown reason, the data from July 11th at 16 :00 to July 12th at 15 :00 are missing, but fortunately there were no drone measurements during this period of time.

Ref	NOV-FE-0899-NT-102		
Issue	2	Date	03/04/23
Rev	1	Date	17/04/23
Page	41/55		

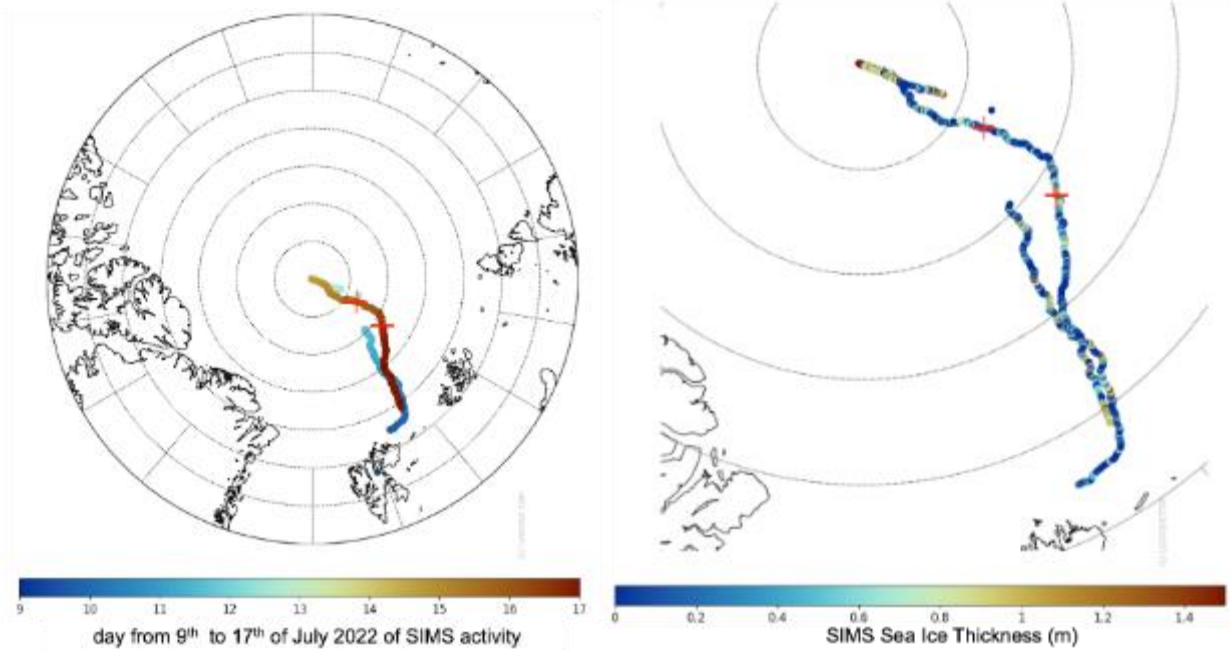


Figure 41 - The image on the left shows the trajectory of the ship recorded with the SIMS data over sea ice, the colour represents the date in day for July: the data were acquired from July 9 to 17 (with a nearly 24h of interruption from July 11 at 16:00). The image on the right shows the sea ice thickness measured by the SIMS along the trajectory. The red crosses show the places where we made freeboard measurements with the drone on the way back, once July 15th and twice July 16th.

We converted the CSV files into a NetCDF file that covers the entire mission. This 1.5 MB file contains 620083 measurements (1 per second), each associated with 4 parameters: time, lon, lat and SIT. The figure below shows the SIT value as a function of time during the 10 days among the ice. The white spaces correspond to when the sensor is off, and the periods with little variability correspond to when the boat is stopped.

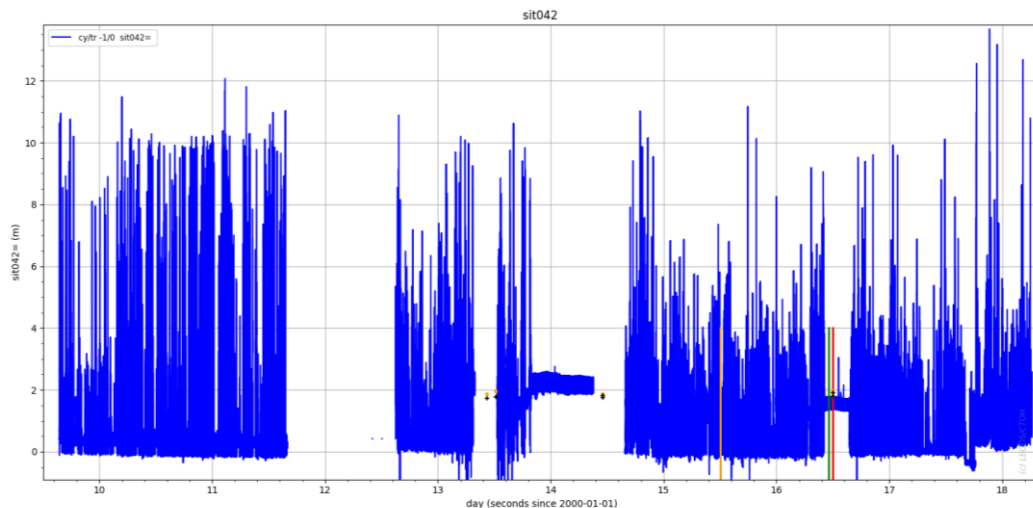


Figure 42 - Sea Ice Thickness measured by the SIMS at 1Hz. The first hole in the data around July 12th is an interruption of the SIMS (for unknown reason). The following ones correspond to stops of the ship. The more stable measurements around the 14th and end of 16th also correspond to stops of the ship over ice floes. Globally we can observe very large variations, up to 10 meters, which probably come from ridges. The 3 coloured vertical lines correspond to the drone measurements.

The following figure shows a zoom of the previous one around July 15 at 12:00, where we made some drone measurements. This zoom shows that the mean value of the SIT is much lower than the peaks that dominate the previous overview.

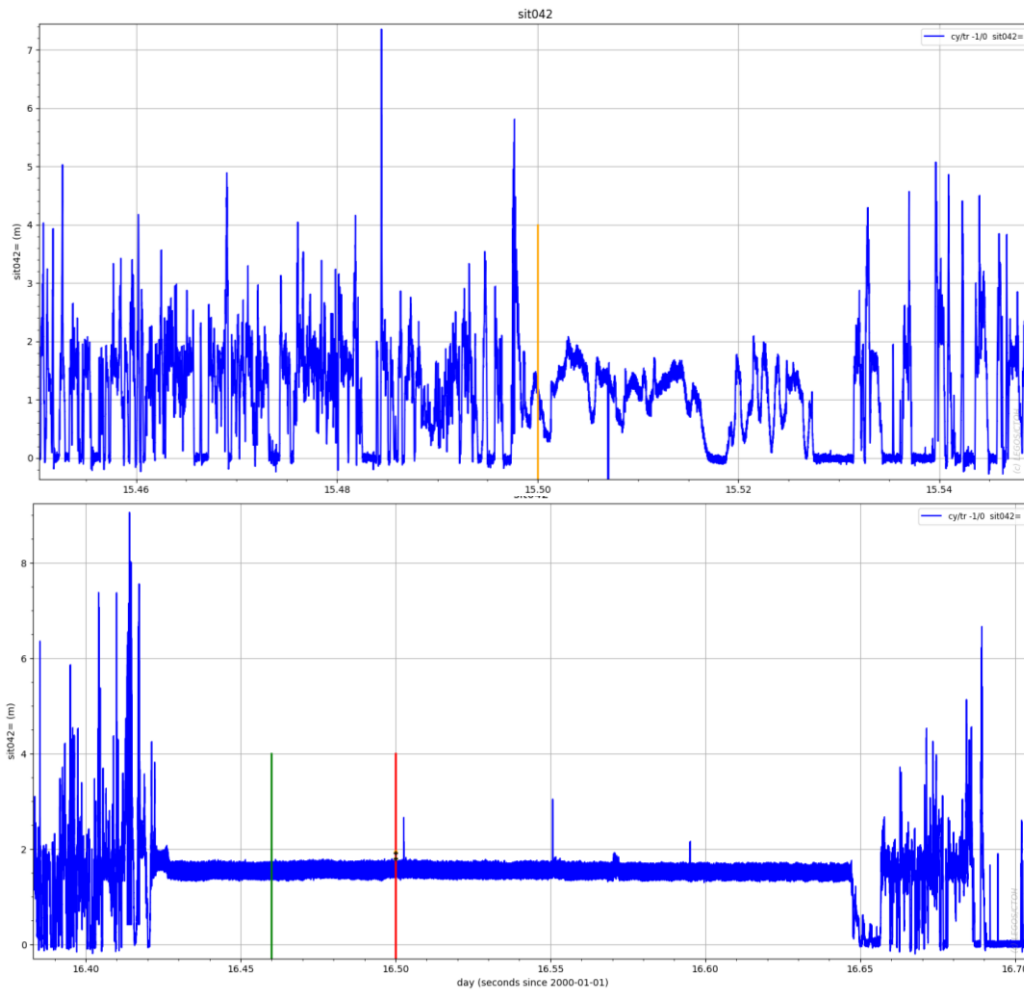


Figure 43 - Zoom of the previous Figure around July 15 at 12:00 and July 16 at 11:00 and 12:00 when we made drone measurements. Whereas some peaks reach more than 4 meters, the mean SIT value is about 1.5m to 2m. The leads can be easily distinguished with SIT=0.

3.4.1.3. Field datasets

6 ice samples were taken during the stops of the ship on the ice pack. The corresponding ice thickness measurements are listed in the table below. These values have been plotted on Figure 41 of the SIMS measurements as black cross for the SIT and small orange dots for SIT+SD. Samples #5 and #6 were taken on July 16 around 12:00 and thus they correspond to the freeboard measurements by drone on that day. They can be seen also on the zoom.

sampling	#1	#2	#3	#4	#5	#6
day since 2022/07/01	13.43	13.512	14.458	14.458	16.5	16.5
longitude	75.3007	75.3007	14.3917	14.3917	56.9757	56.9757
latitude	89.8694	89.8694	89.9804	89.9804	85.5532	85.5532
SIT	1.74	1.79	1.77	1.83	1.92	1.80
SD	0.13	0.17	0.90	0.90	0.00	0.00

Ref	NOV-FE-0899-NT-102		
Issue	2	Date	03/04/23
Rev	1	Date	17/04/23
Page	43/55		

3.4.2. Freeboard processing from lidar datasets

As shown in the figure below, measuring the freeboard at the water/ice boundary is relatively easy as long as the water and ice are seen simultaneously. Unfortunately, this measurement is not representative of the freeboard of the whole floe because the edge of the floe may be eroded or on the contrary present mounds resulting from impacts with other floes. It is therefore necessary to measure the freeboard, i.e. the height of the ice relative to the water away from the edge.

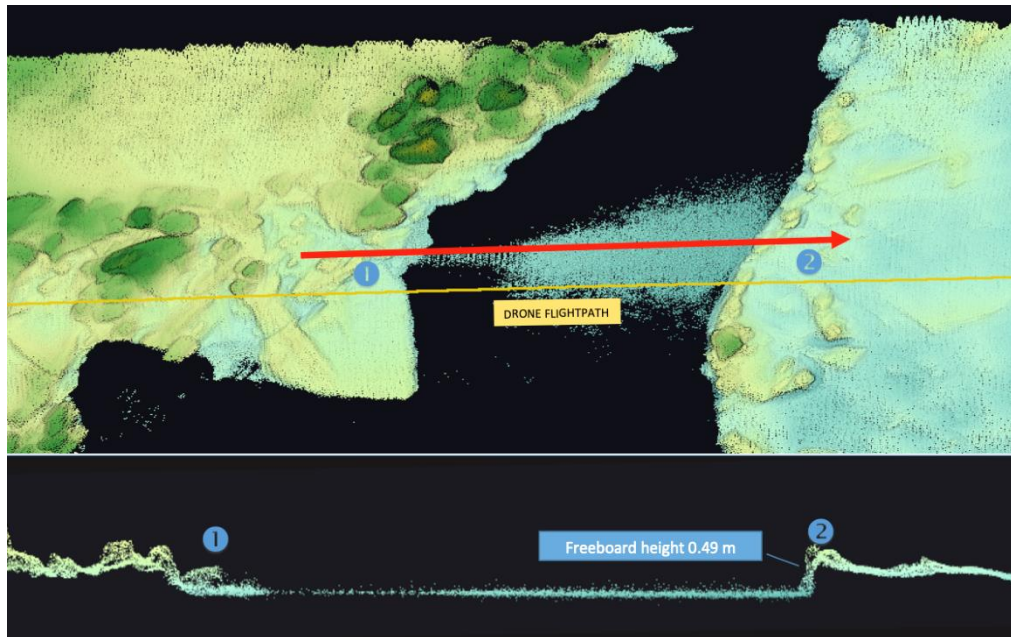


Figure 44 - A cross section over a lead between two floes. The 3D model allows to measure quite precisely a freeboard at point 2 of 49cm. The black surfaces correspond to the open water of the leads. Because of the specularity of the water only nadir shots can return back to the sensor (the points below the red arrow between the 2 floes).

We can also observe on this same scene that the 3D scanner has no return from the water if it is not vertical to the surface. This is a well-known phenomenon that can be explained by the high specularity of water that reflects the laser wave at an angle symmetrical to the angle of reception relatively to the vertical axis. In order to dispose of reference measurements on water, we consider only the measurements near the nadir with angles of less than 0.01 radians (0.6 degrees). To do this, it is sufficient to exploit the firing angle parameter which is provided in the YellowScan data. The black dots in the middle the figure (with the superimposed intensity of the backscatter) below shows the selected points close to the vertical of the drone track.

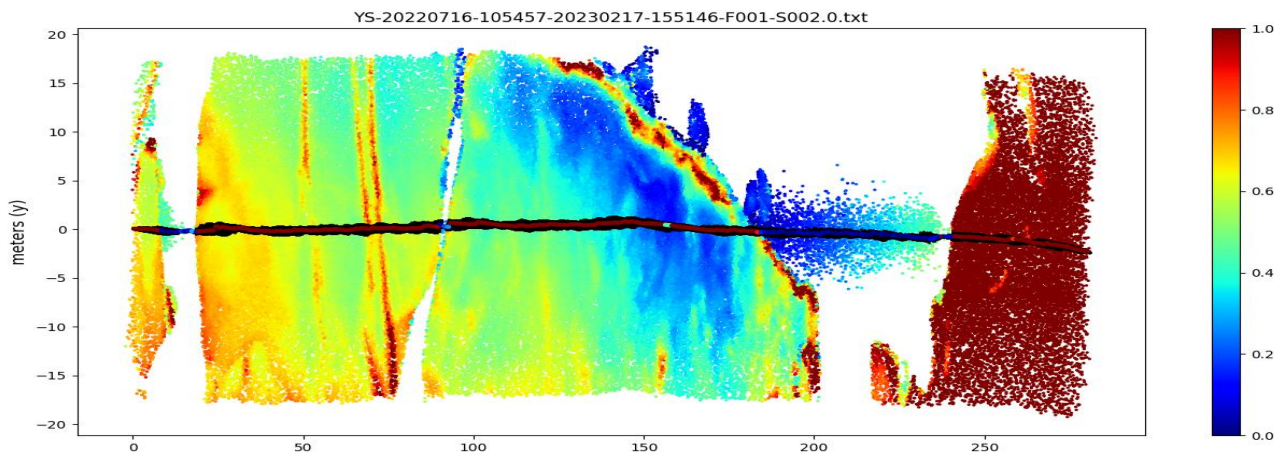


Figure 45 - A 3D scene from a top view. Only the black dots that correspond to the vertical of the drone path are kept to measure the freeboard. The colour bar represents the height of the surface in meters. The intensity of the backscatter is superimposed over these black dots.

The dark section that corresponds to the nadir measurements is shown after filtering from the side in the following Figure. The height of the surface is the red line and we have juxtaposed the intensity of the returned signal measure by the sensor in purple. This confirms the very low intensity returned from the water within the leads. The height curve in red shows strong incongruities on the water levels in the leads while between about 180m and 240m one can expect a constant level. This slope is probably due to the quality of the internal positioning system of the YellowScan sensor. Indeed, YellowScan prefers to rely on the 3D reconstruction of the scene by merging the point clouds rather than on the position of the sensor, which only plays a secondary role. But 3D reconstruction is impossible for a deformable 'object' such as the ice pack.

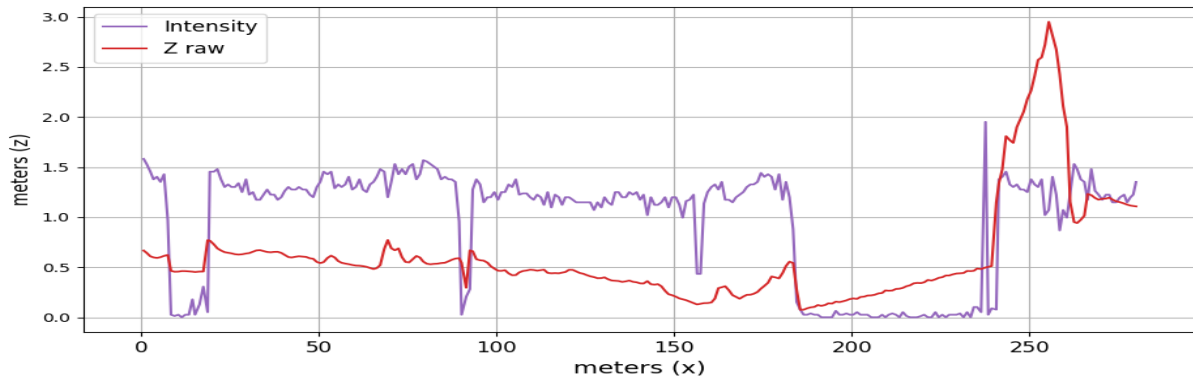


Figure 46 - The red line corresponds to the height of the surface along the drone path shown in previous Figure 45. The purple line corresponds to the backscatter of the surface. Three leads can be easily seen which correspond to the 3 portions of minimum intensity. We can also observe that the first lead is at about 50cm height, the second tiny one at about 35cm and the large last one raise from 5cm to 50cm!

The results obtained with the Vortex.io sensor during the March mission in Upernavik show that this level of positioning problem is specific to the YellowScan. On the other hand, the flatness of the water in the previous figure and the repeatability of the ice patterns (Figure 37) suggest that the laser measurements are not in question.

In order to be able to exploit these laser measurements, we use in following the water level as a height reference. Water surfaces are identified by the backscatter intensity measured by the laser sensor. This corresponds to the blue points juxtaposed on the purple intensity curve in the following figure and on the red curve of heights. By a spline interpolation of these points along the path we obtain a new height reference at water level in blue. The green curve corresponds to the red curve brought back to this new reference, that is to say the height of the floes relative to the height of the water, and thus the freeboard sought.

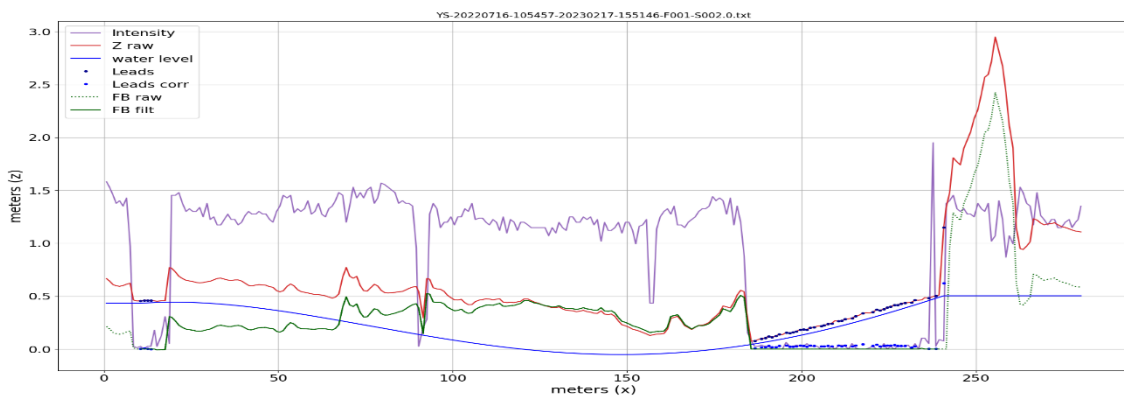


Figure 47 - Water surfaces, identified by the backscatter intensity level, are indicated by the blue dots. These points are used to interpolate the water level along the trace. The corresponding blue line defines the new height reference which aims the red curve to the green curve. The green curve represents the desired freeboard. The dotted parts at the beginning and the end of this curve are ignored because there is no information about the drift of the altitude of the drone before the first lead and after the last lead.

Only the portions of the trace between 2 leads can be considered. Indeed we cannot know the evolution of the altitude beyond the leads. For example, in the case of the figure above we cannot know if beyond the 240m the position has continued to drift upwards or if it has stabilized. This is why we do not consider the freeboard measurement beyond this last lead and it is represented in dotted lines.

By applying this correction to all the points acquired along the trajectory, including off-nadir, we obtain the corrected height map below, to be compared with the map before correction in Figure 45.

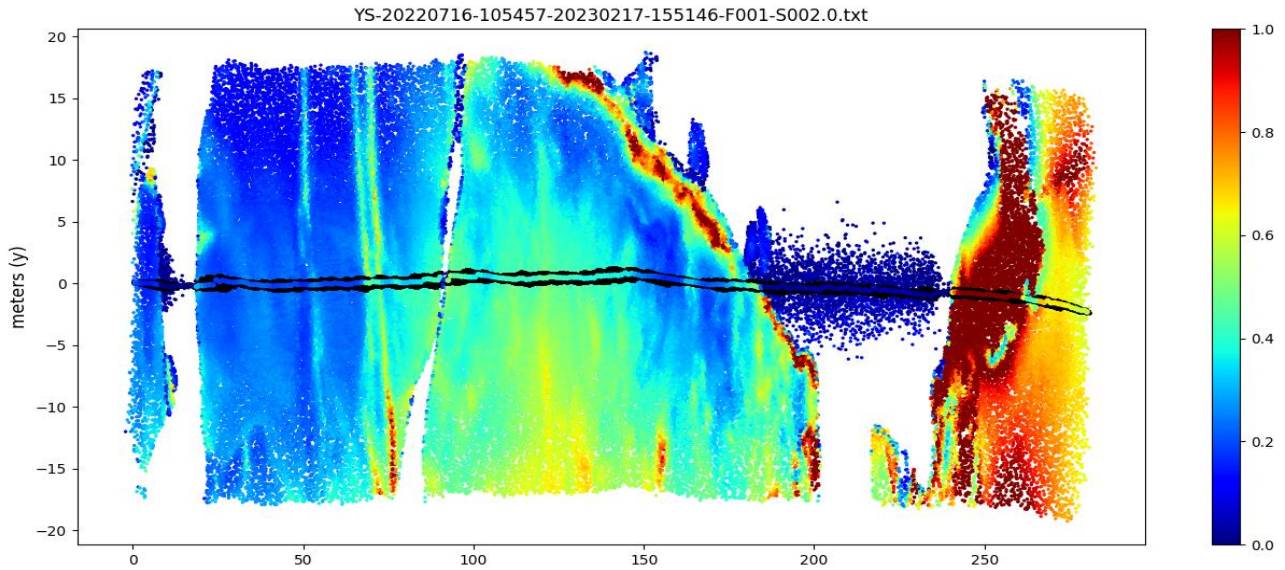


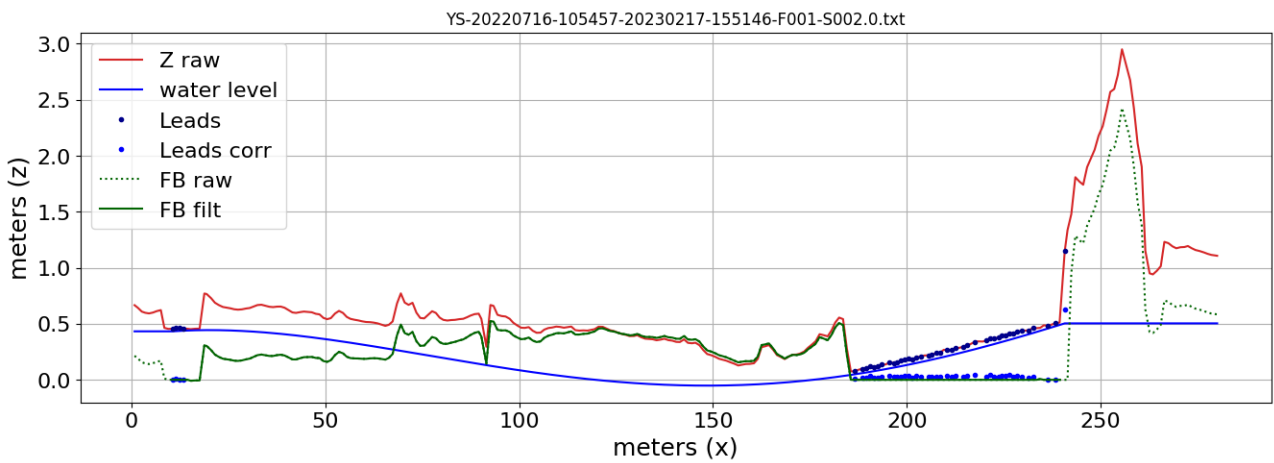
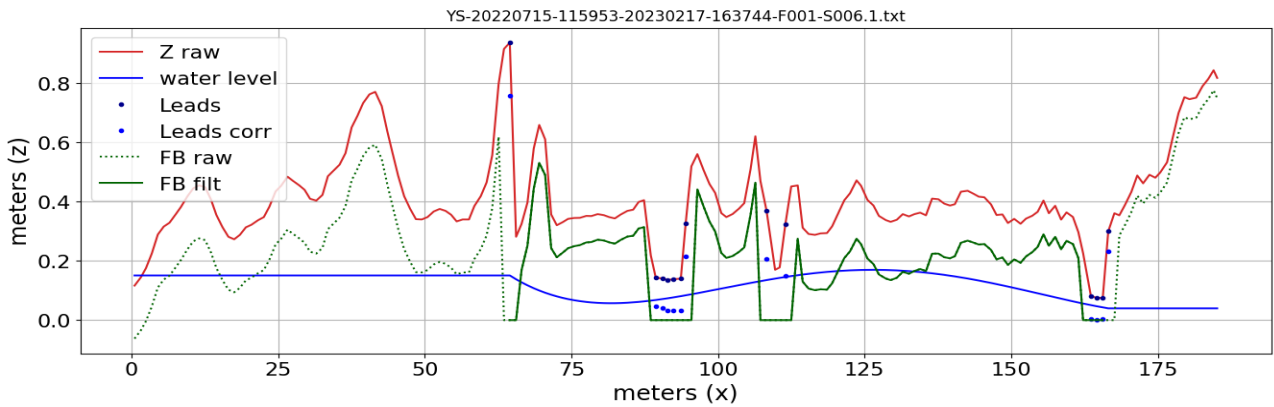
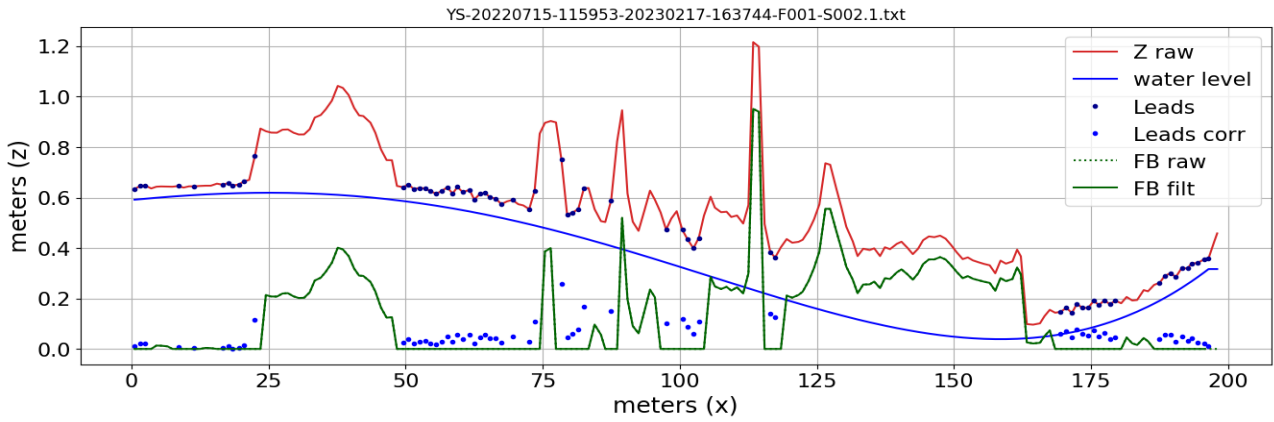
Figure 48 - The corrected height map to be compared to the original one Figure 45. The data selected to compute the correction are in black, with the height along the corrected track in colour. We observe the good continuity between the track and the measurements off-nadir.

The need to have leads on both sides of the floe measurements and the limited number of measurements observed on the water considerably reduced the number of exploitable tracks. Nevertheless, there are still 13 traces spread over the 3 flight sequences for which we provide the statistics in the table below.

date hour	ref	max	mean	std	median	MAD
15 12h	2.1	0.95	0.252	0.155	0.264	0.056
	4.1	0.95	0.289	0.205	0.262	0.148
	6.1	0.53	0.241	0.082	0.238	0.032
16 11h	2.0	0.52	0.299	0.110	0.316	0.096
	6.1	0.80	0.242	0.161	0.189	0.056
	1.1	0.51	0.214	0.096	0.203	0.040
16 12h	1.2	0.77	0.318	0.186	0.369	0.131
	2.1	0.66	0.314	0.157	0.305	0.106
	6.2	0.54	0.237	0.094	0.231	0.052
	7.1	0.43	0.248	0.109	0.261	0.096

Table 1 - Freeboard characteristics for 10 drone tracks

The following figures show several illustrations.



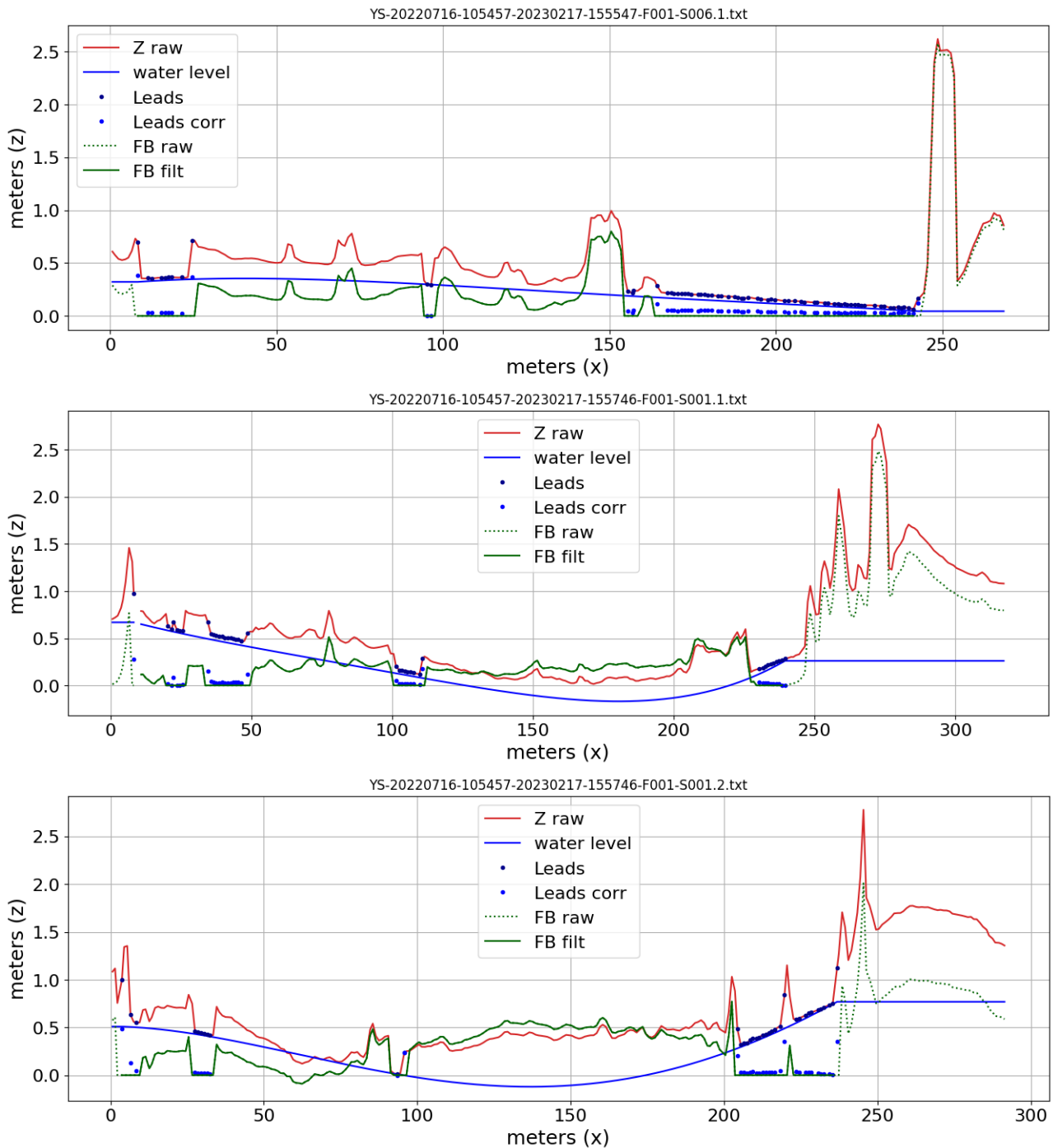


Figure 49 - The heights obtained with the YellowScan along the drone tracks are in red, with the points identified as lead measurements in blue. The blue line represents the interpolated water level that is used to correct the red height curve. The corrected curve is in green. This green curve being the height of the floes relatively to the sea level, it represents directly the freeboard of the ice

Finally, the freeboard can be converted to sea ice thickness using the equilibrium equation with the hypothesis that the laser does not penetrate the snow and measures a total freeboard ($FB_{ice} + SD$):

$$SIT = [\rho_w \cdot FB_{laser} + (\rho_s - \rho_w) \cdot SD] / (\rho_w - \rho_i)$$

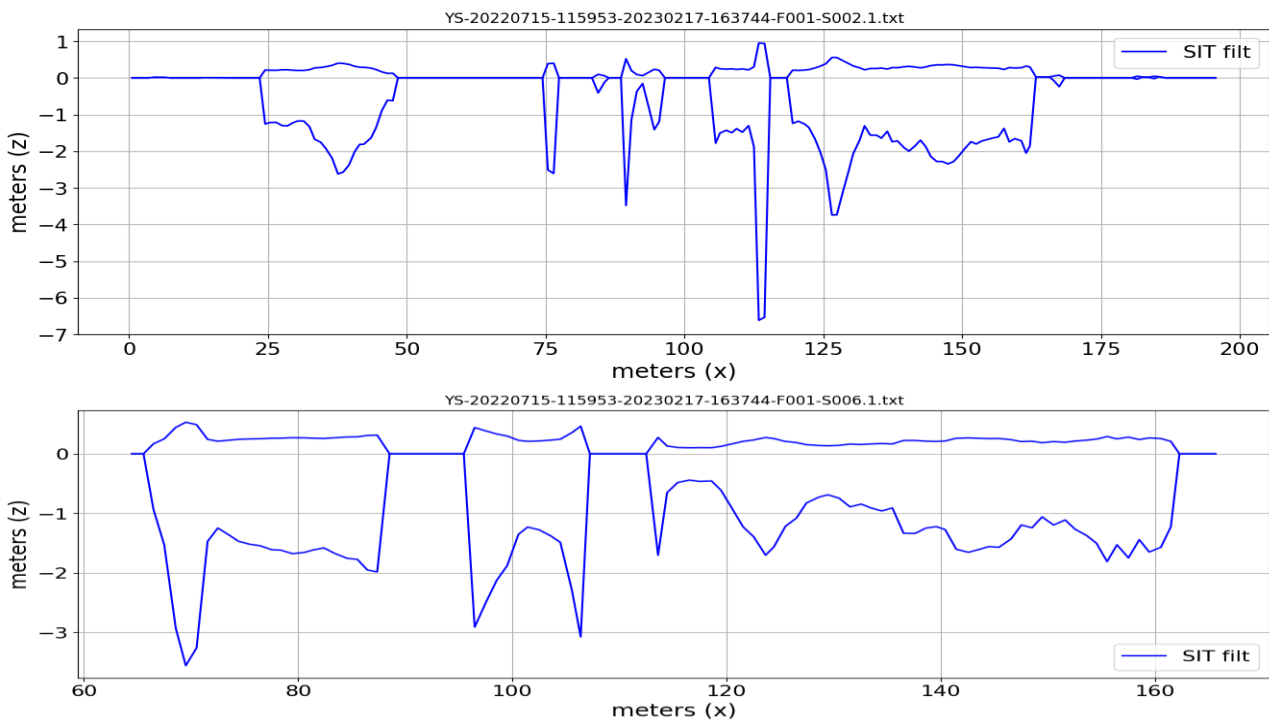
with the following values: $\rho_w = 1.024$ $\rho_i = 0.900$ $\rho_s = 0.300$ and $SD = 0.05$

The snow depth of 5cm has been chosen following the field measurements. The density of the ice is the mean between first year and multi-year ice as the ice encountered was a mixed of 1 year and 2 years old ice.

date hour	ref	max	mean	std	median	MAD
15 12h	2.1	7.56	1.804	1.254	1.886	0.462
	4.1	7.56	2.105	1.680	1.874	1.220
	6.1	4.09	1.699	0.677	1.676	0.261
16 11h	2.0	4.03	2.184	0.891	2.320	0.795
	6.1	6.30	1.704	1.326	1.272	0.462
	1.1	3.95	1.479	0.791	1.380	0.327
	1.2	6.06	2.385	1.444	2.751	1.083
16 12h	2.1	5.15	2.303	1.295	2.224	0.879
	6.2	4.15	1.667	0.765	1.612	0.432
	7.1	3.25	1.756	0.902	1.863	0.794

Table 2: Sea Ice Thickness characteristics for 10 drone tracks

The following figures illustrate few cases of Sea Ice Thickness deduced from the freeboard measured with the drone and the Equation above. We observe a good coherency with the SIMS measurements with a mean sea ice thickness of about 1.8m and which can reach locally more than 7m.



Ref	NOV-FE-0899-NT-102		
Issue	2	Date	03/04/23
Rev	1	Date	17/04/23
Page	49/55		

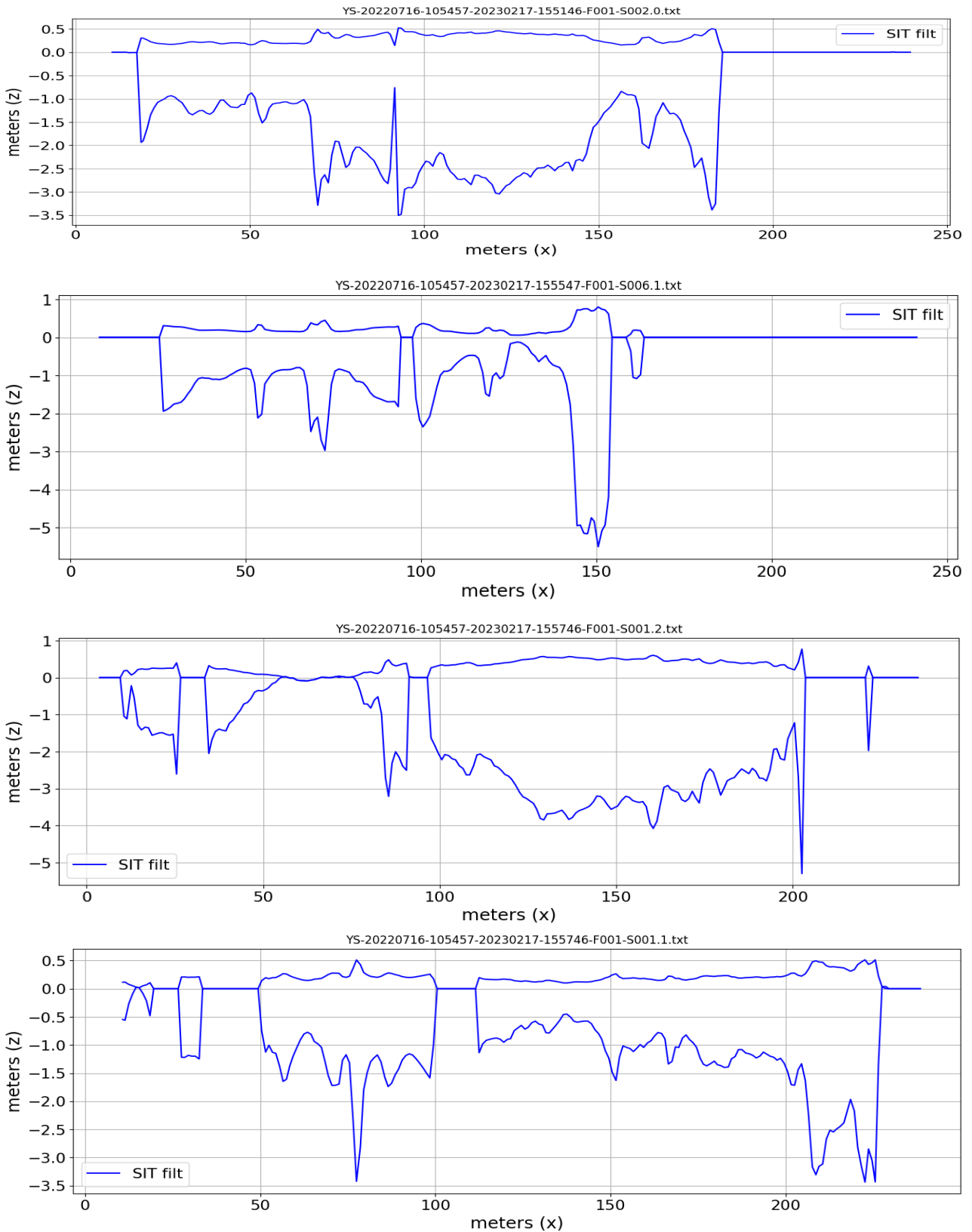


Figure 50 – The Sea Ice Thickness is deduced from the freeboard measurement (top blue lines) and the hydrostatic equation which provides the SIT and the draft (bottom blue lines)

In the two following figures, we have superimposed SIMS SIT measurements with drone SIT estimations for respectively the vessel stops of July 15th and July 16th. We observe a good coherency with the SIMS measurements, and a mean sea ice thickness of about 1.8m and which can reach locally more than 7m.

Ref	NOV-FE-0899-NT-102		
Issue	2	Date	03/04/23
Rev	1	Date	17/04/23
Page	50/55		

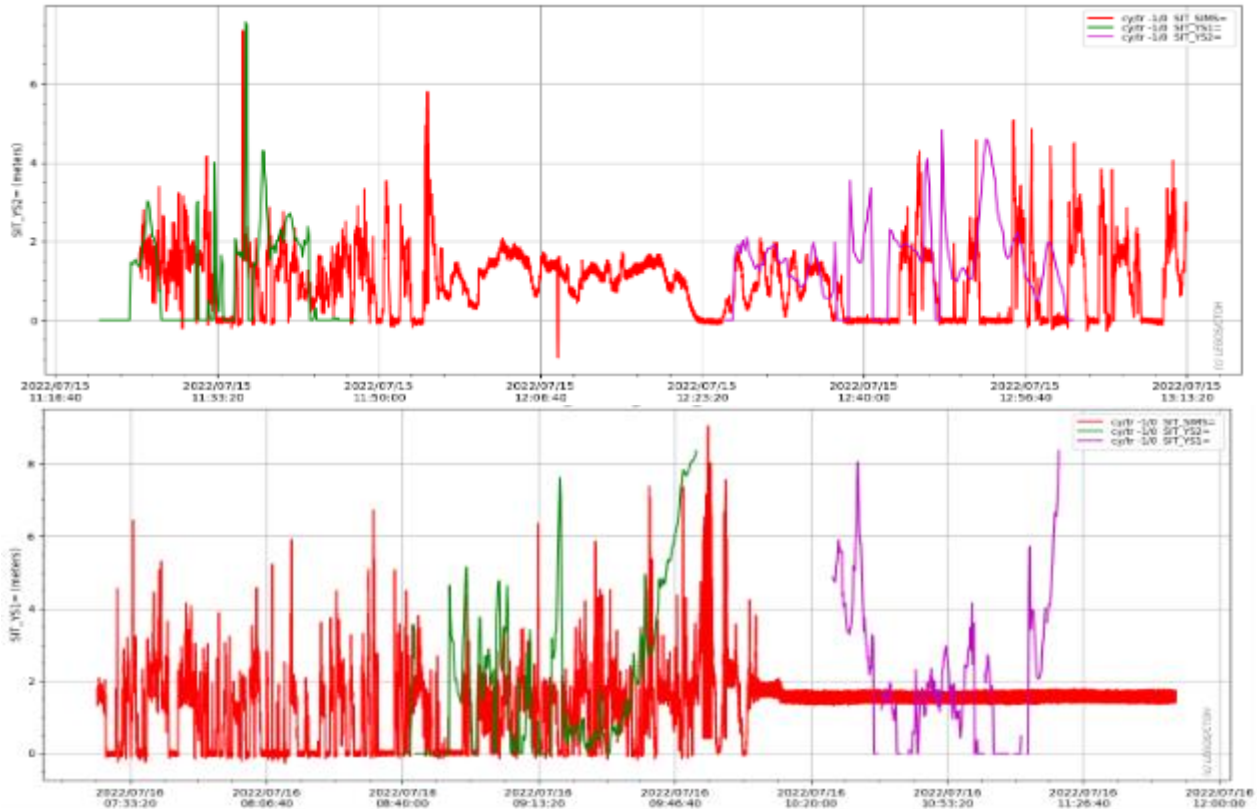


Figure 51 - The Sea Ice Thickness measured with the SIMS is in red. The green and purple curves have been deduced from drone measurements. They cannot fit directly because the trajectories of the vessel and of the drone are not the same (for validation purpose it would worth to fly the drone ahead the vessel). In fact, the drone measurements have been done around the vessel when it was stopped. It explains for example why the SIT in red is constant around 1.8m on the right part of the second plot. The SIT variation must be observed on the left part of this same plot. The super-impositions allow to see that the SIMS and the YellowScan observe similar ice values and dynamics.

SENTINEL-3 TOPOGRAPHY MISSION ASSESSMENT THROUGH REFERENCE TECHNIQUES (ST3TART)	Ref	NOV-FE-0899-NT-102		
	Issue	2	Date	03/04/23
	Rev	1	Date	17/04/23
	Page	51/55		

3.4.3. Discussion

The results presented here show a very good consistency between the 3 types of measurements made during the mission: with the SIMS, the field measurements and the drone. The exploitation of the YellowScan data proved to be a bit difficult due to the very poor positioning of the sensor. This limited us to small sections of trajectories, of the order of 250m, bounded by leads. Even so, the very consequent variations of the water level (up to 50cm of difference in level on 50m of trajectory!), makes the interpolation of the water level a little risky.

The use of a sensor equipped with a good positioning system such as that of Vortex.io makes it possible to limit this problem considerably, as it was demonstrated during the March mission to Upernavik. Studies are underway in collaboration with the GRGS group of the Midi-Pyrénées Observatory to determine the achievable accuracy of the UAV altitude without using a baseline. This precision will condition the uncertainties on the floe heights as a function of the distance to the nearest leads, and thus allow to increase the dimensions of the floes that can be measured in a sufficiently reliable way.

On the other hand, the YellowScan has allowed to appreciate the impressive quality of the laser measurements on the ice pack (see Figure 37 and Figure 38). We can also note that only nadir measurements (less than 0.01 radians) of the 3D scanner were used to measure the freeboard because the measurements with an angle greater than 1° have no return on the water in leads. These measurements on the water are essential since they serve as a reference for the measurement of freeboard. Thus, the Vortex.io sensor, which has 8 beams close to nadir, is quite appropriate for this type of measurement and has the advantage of being more compact and certainly less expensive (60k€ for the YellowScan model that we used).

To conclude for the drone measurements, we recall that the primary objective of this mission was to demonstrate the feasibility of deploying a drone from a ship to measure the freeboard of the pack ice, to establish a list of difficulties and to determine the possible workarounds. This operational assessment is developed in the TD-12 report. As can be seen from TD-12, but also from the results presented in this report, we can affirm that the use of drones for this type of measurement is entirely realistic and can fill the gap between field and airborne measurements.

However, a certain number of actions are still necessary to make this method easily usable by technicians on ships or polar stations, without systematically calling on a professional drone pilot. This is a condition to allow a quasi-systematic deployment on icebreakers or in polar stations in order to increase the spatio-temporal coverage of sea ice measurements. Other developments, such as the use of fixed-wing UAVs of the VTOL type (Vertical Take-Off and Landing), may allow the implementation of larger-scale missions by increasing the spatial coverage thanks to their much greater accessible ranges.

Finally, it is important to note the quality of the SIMS measurements, a sensor designed by Christian Haas of AWI. This sensor has already been deployed on a dozen icebreakers for their own needs: in addition to the Commandant Charcot, it is also deployed on the following ships: Polarstern, Lance, Kronprins Hakon, MV Arctic, Kapitan Dranitsyn, Aurora Australis, Shirase, Nuyina, Oden, and others (see Christian Haas for more information). This sensor has multiple advantages: it does not require an operator during the measurements (only for its deployment and time to time calibration of the zero), it delivers real-time measurements, it is useful for ice navigation, it is robust and its cost is limited (the sensor is about 20k€ and the operating cost is almost zero). Perhaps it could also be considered to add a snow radar on the SIMS, such the one used by NORCE team from University of Tromso on their drones (contact: Robert Ricker). We therefore recommend actions to promote its deployment and set up agreements with ship operators to recover the data.

Ref	NOV-FE-0899-NT-102		
Issue	2	Date	03/04/23
Rev	1	Date	17/04/23
Page	52/55		

4. Comparison of S3 data to campaign data

To be provided when we have the S3 baseline processing adapted for sea ice conditions.

- 1) Development of comparison procedures adapted to each type of measurement.
- 2) Comparison of the measurements with S3 STM Land data.
- 3) Evaluation of the contribution, in terms of S3 Cal/Val, of these in-situ and spatial measurements.

Ref	NOV-FE-0899-NT-102		
Issue	2	Date	03/04/23
Rev	1	Date	17/04/23
Page	53/55		

5. Conclusions

We present here the first conclusions concerning the different types of measurements carried out on the ice pack during the project. More general recommendations will be developed in the roadmap.

5.1. Airborne measurements

Airborne measurements of the ice pack have been carried out regularly for many years by NASA (OIB), ESA (CryoVex) generally in collaboration with other institutes, including in particular DTU and AWI. It is essential that these measurements can continue. We make here a quick review of the 2022 achievements and recommended developments.

During March 2022, expedition measurements were made in Baffin Bay under the tracks of the S3A and S3B satellites. The ALS laser scanner, one of the most used sensors to measure the freeboard, provided a modal total freeboard FB_{total} of 10cm to 20cm which is what is expected in this area. We could not compare these results with S3 because the thematic data dedicated to sea ice are not yet available.

However, these measurements are consistent with those made during the deployment of the Ice-T buoy. We have indeed noted on this occasion a snow depth of 6 cm with an ice thickness of 55 cm and an ice freeboard of the order of 4cm to 5cm, or a total freeboard of 10cm to 11cm.

We do not yet have the Ka and Ku radar freeboards. This problem illustrates the widespread problems of latency in data processing between expeditions due to the lack of means devoted to post-processing, validation, documentation and distribution of data.

But one of the most critical points is the lack of snow radar. Without snow depth measurements, it is not possible to compare the total freeboard measured by lidar with the radar freeboard measured by the S3 or CryoSat satellites. It will also not be possible to evaluate the ability to estimate snow depth by Ka Ku difference, either by airborne, by comparison of S3 or CS2 with Saral or in preparation for CRISTAL.

5.2. Ice-T measurements

The Ice-T buoy performed well during its 2 weeks limited life-time, which ended abruptly most likely due to a polar bear attack. The new innovative miniature FMCW radars operating at 120 GHz and 24 GHz to improve capabilities of the snow depth measurements of the Ice-T buoy were tested in the Pyrenees before deployment in Baffin Bay. At nadir looking observations in Baffin Bay in particular, the 120 GHz shows promising results to obtain snow depth estimates, and provides information on snow fall.

In the absence of additional snow depth information coincident with the Ice-T operational period, an inter-comparison between the snow depths from the Ice-T buoy and re-analysis ERA5 was performed. The inter-comparison study concluded that the ERA5 re-analysis of snow depth was not reliable over sea ice in this region, and did not notably capture one snow fall event during deployment. This result highlights the importance of snow measurements on pack ice, an ECV that is still very poorly understood.

A second Ice-T buoy was to be deployed at the North Pole. The first option in spring 2022 from the Russian ice camp Barneo was not possible due to the geo-political situation. The second option to deploy an Ice-T buoy from Le Commandant Charcot was not successful, due to damage during transport, and the deployment had to be cancelled.

Thus, while the miniature radars for snow depth measurements are promising, they still need further tests. If the snow depth radars turn out to be successful, the Ice-T buoy will provide all the necessary information to characterize the ice: snow depth, ice thickness and sea ice drift.

SENTINEL-3 TOPOGRAPHY MISSION ASSESSMENT THROUGH REFERENCE TECHNIQUES (ST3TART)	Ref	NOV-FE-0899-NT-102		
	Issue	2	Date	03/04/23
	Rev	1	Date	17/04/23
	Page	54/55		

5.3. Drone measurements

Drones are developing extremely rapidly and their flexibility of deployment will probably make them an essential measurement medium. However, polar and oceanic conditions pose specific problems, in particular related to climatic conditions, flight control and positioning accuracy. Within the framework of this project, we have deployed two expeditions allowing us to confront different conditions. The first one took place on the coast of Baffin Bay at the end of the winter, and the second one from an icebreaker in the North Pole at the beginning of the summer.

For the Baffin Bay mission, the drone was equipped with a Vortex.io lidar and a camera. It has been successfully tested in cold conditions, i.e. for temperatures down to -13°C , at latitudes of about 72.5°N . This is a first important step although in the Arctic Winter the temperatures can typically reach down to -30°C . For instance, a drone experiment conducted at about the same period outside Eureka in -30°C failed to work. Thus, methods of heating the vital elements could be useful in extreme cases.

Despite the high 82.5° latitude of the Baffin Bay the GNSS solutions show high performance, with 3.4 mm standard deviation with GNSS base station on solid ground, and with a lightly degraded performance of 1.4 cm standard deviation with the GNSS base station on the sea ice. This is mainly due to tidal elevation changes of the base station.

The lidar performed excellently, and only few measurements have been lost due to high pitch angle (> 2 degrees). The standard deviation of lidar elevation measurements is directly linked to the surface roughness and not to the displacement of the drone during the flights. The surface roughness is an important input parameter for development of radar satellite altimeter physical retracers, which should be further exploited in the future.

Some of the drone images of the sea ice were overexposed, in particular in cases with presence of leads. We further conclude that the NDWI difference index is successful for lead detections.

It could be interesting to install a camera with larger FoV to provide overlap between the tracks at the lower altitude flown by the lidar equipped drone (30m vs 100m).

For the second expedition to the North Pole, the Vortex.io sensor was unfortunately not available. However, the company YellowScan was willing to lend us one of their 3D scanners.

The primary objective of this 2nd mission was to determine the feasibility of deployment from an icebreaker and to establish an exhaustive list of difficulties. Contrary to our fears, we did not encounter any interference problems with the ship's electronics nor any problems controlling the drone because of the North Magnetic Pole located 400km away. However, we know that a drone crashed at the Dumont d'Urville station located at 300km from the South Magnetic Pole. This remains a point to be monitored. On the other hand, the control interface of the drone, in Mercator projection, proved to be unusable near the geographic pole and the take-off and landing operations from a ship are very delicate operations requiring a professional pilot. There are however techniques to automate these phases of flight.

The most critical point concerns the precise location of the drone and in particular its altitude. The method developed by YellowScan to reconstruct a 3D model from point clouds does not require precise localization and therefore the localization integrated into the system is very deficient and does not propose to recover the GNSS data for post-processing. In any case, to be able to measure the freeboard of the pack ice over significant distances (a few kilometres), it is essential to obtain a positioning with an accuracy of the order of a centimetre. This accuracy is generally obtained thanks to the presence of a fixed reference base, as was the case during the first mission. However, this approach is not applicable from a ship which, even when stationary, is subject to drift due to wind and currents. However, innovative GNSS post-processing techniques such as PPP (Precise Point Positioning) theoretically allow to reach this kind of accuracy. We are currently conducting a study with the GRGS group of the Observatoire Midi-Pyrénées in Toulouse around their GINS software using the measurements made in Baffin Bay. We hope to obtain first results before the final review of this project.

In spite of these difficulties, we were able to make freeboard measurements of very satisfactory quality. As for the first mission, the laser sensor proved to be very efficient. In the absence of precise positioning, we relied on the height of the water in the leads to define the floe height reference. These results have been validated against the other ice measurements made during this mission: the field measurements and the measurements delivered by an Electro-Magnetic Sensor SIMS located at the front of the ship.

SENTINEL-3 TOPOGRAPHY MISSION ASSESSMENT THROUGH REFERENCE TECHNIQUES (ST3TART)	Ref	NOV-FE-0899-NT-102		
	Issue	2	Date	03/04/23
	Rev	1	Date	17/04/23
	Page	55/55		

In parallel to these two missions, NORCE from Tromso University (contact: Robert Ricker) has carried out the first snow depth measurements using a drone with very demonstrative results.

The use of UAVs is still a young approach to carry out FRM measurements, but these missions have demonstrated its feasibility and there is no doubt that this technique has a strong potential that will develop further in the near future. This would allow to fill a gap between field and airborne measurements, both in terms of coverage and accuracy, and this with much lower risk or cost. We will discuss in the context of the Roadmap the actions that can be considered to accelerate this trend.

5.4. Other techniques of measurements

These missions also gave us the opportunity to evaluate two other techniques for measuring the thickness of the pack ice that we believe are suitable for FRM-type measurements.

The first one concerns the SIMS (Sea Ice Measurement System) sensor which consists of an EM31 type electromagnetic sensor to measure the draft of the pack ice combined with a sonar to measure the freeboard. This sensor, suspended at the bow of the Commandant Charcot, delivers in real time the thickness of the pack ice to the command bridge of the ship. It is therefore already an operational system. We have been able to retrieve and evaluate these data, which are of extremely good quality. This system, designed by Christian Haas (AWI), has been deployed on about ten icebreakers. It would be interesting to see if these data could not be collected systematically for scientific purposes and altimetric validation. It could also be interesting to encourage the deployment of SIMS in a systematic way, and, why not, to associate a snow radar with SIMS.

A second approach, developed by Frédéric Vivier of LOCEAN, is to measure the thickness of ice broken and rolled on its side by the ship using a stereoscopic bench. This technique is inexpensive and relatively simple to implement and would provide quantitative data instead of the visual estimates made, for example, in the ASPECT project. This approach is being evaluated at LOCEAN.

5.5. Overall conclusion

In conclusion, in this study we have evaluated a wide variety of approaches to measuring freeboard and/or pack ice thickness. Some offer measurement qualities compatible with FRM measurements. We have also evaluated the difficulties and their potential solutions. Their relative maturity levels and the actions that can be implemented will be the subject of the Roadmap.